JOURNAL OF GEOPHYSICAL RESEARCH, VOL. 88, NO. A8, PAGES 6143–6163, AUGUST 1, 1983

Electron Precipitation and Related Aeronomy of the Jovian Thermosphere and Ionosphere

J. H. WAITE, JR.

Space Science Laboratory, NASA Marshall Space Flight Center
Huntsville, Alabama 35812

T. E. CRAVENS, J. KOZYRA, A. F. NAGY, AND S. K. ATREYA

Department of Atmospheric and Oceanic Science, Space Physics
Research Laboratory, University of Michigan,
Ann Arbor, Michigan 48109

R. H. CHEN

Center for Radar Astronomy, Stanford University,
Stanford, California 94305

Voyager ultraviolet spectrometer (UVS) measurements provided the first unassailable evidence for particle precipitation in the Jovian atmosphere. Strong Lyman and Werner band emissions at high latitudes indicate particle precipitation energy fluxes of about 10 ergs cm^{-2} s^{-1}. On the other hand dayglow Lyman and Werner emissions at mid- and low-latitudes may indicate additional particle precipitation fluxes on the order of 0.3 ergs cm^{-2} s^{-1} at all latitudes. Such particle precipitation can have significant aeronomical effects on the Jovian thermsophere and ionosphere. A one-dimensional theoretical model is used to study these effects for the case of electron precipitation, although ion precipitation produces similar effects. Diffusion equations are solved for all the major neutral species and for H^+, and photochemical solutions are given for the short lived ions. These neutral and ionospheric components of the model are coupled with the electron and ion energy equations and a two-stream electron transport code that calculates the energy deposition of precipitating electrons (considered to be the precipitating particles) and photoelectrons. An independent calculation of the vertical neutral temperature is also obtained. The results of the model calculations can be broadly categorized as effects of electron precipitation (1) on the neutral composition and temperature of the thermosphere, and (2) on the composition and structure of the ionosphere. Auroral electron precipitation by 10-keV electrons with a total energy flux of 10 ergs cm^{-2} s^{-1} produces 4.7×10^{11} H atoms cm^{-2} s^{-1} and 5 ergs cm^{-2} s^{-1} of heat, over 2 orders of magnitude larger than solar EUV processes that produce 3.3×10^9 H atoms cm^{-2} s^{-1} and 0.03 ergs cm^{-2} s^{-1} of heat. Thus, Jovian auroral H production coupled with aurorally driven meridional winds in the thermosphere can possibly explain the high concentration of atomic hydrogen in the low-latitude Jovian upper atmosphere. Furthermore, aurorally produced changes in composition can create important feedback which affects the relative airglow efficiencies and heating rates in the high-latitude thermosphere. In addition, ionization and vibrational heating of H_2 from precipitation processes appear to play a central role in determining the structure of the high-latitude ionosphere. Theoretical fits to the Voyager radio occultation electron density profiles at high latitudes suggest a 10-keV electron aurora with an energy flux of 10 ergs cm^{-2} s^{-1} coupled with a height-dependent H_2 vibrational temperature that reaches 3000 K in the topside ionosphere.

1. INTRODUCTION

The existence of diffuse aurora on Jupiter has been suspected for quite a few years; although, until recently the observational evidence has been marginal [*Schwitters et al.*, 1968; *Hunter*, 1969; *Dulk et al.*, 1970; *Giles et al.*, 1976]. *Atreya et al.* [1977] also presented evidence for the existence of auroral hot spots at the feet of the Io flux tube. However, the first unassailable evidence for a diffuse Jovian aurora was the Lyman alpha and molecular hydrogen emissions observed by the ultraviolet spectrometer (UVS) on Voyager 1 (V1) [*Broadfood et al.*, 1979]. These emissions were observed in both hemispheres near 65° magnetic latitude. The Io plasma torus maps along Jupiter's magnetic field lines down to invariant latitudes near 65°; therefore, the natural interpretation has been that the plasma torus is to a large extent the source of the precipitating particles responsible for the auroral emissions. Preliminary results from the UVS instrument indicate that the latitudinal extent of the auroral zones maps to the inner and outer edges of the plasma torus suggesting an auroral zone 6000 km wide. Using this auroral width the UVS experiments inferred about 60 kR of Lyman alpha emission and a total of 80 kR of H_2 Lyman and Werner band emissions [*Broadfoot et al.*, 1979, 1981; *Sandel et al.*, 1979]. If the precipitating particles are electrons, this corresponds to precipitating electrons with an energy flux of about 10 ergs cm^{-2} s^{-1} or a global auroral power of about $1\text{–}2 \times 10^{13}$ W [*Waite et al.*, 1980; *Atreya et al.*, 1981; *Yung et al.*, 1982; *Broadfoot et al.*, 1981; *Gerard and Singh*, 1982]. Precipitating ions would require a somewhat lower energy flux to produce the required emissions. Ultraviolet observations of the Jovian aurora have also been made by the International Ultraviolet Explorer (IUE) satellite [*Clarke et al.*, 1980]. *Yung et al.* [1982] used a radiative transfer model for Lyman alpha and H_2 Lyman

Paper number 3A0222.

and Werner band emissions to interpret ultraviolet spectra obtained from IUE and concluded that if the precipitating particles responsible for the emissions were electrons, then the electrons must have energies between 1 and 30 keV.

Ultraviolet emissions do not provide the only evidence for auroral activity on Jupiter. The radio science experiment on Voyager 2 (V2) [*Eshleman et al.*, 1979] measured an electron density profile near 67°S latitude that appears quite different from the other three profiles obtained at lower latitudes, specifically the electron densities are smaller by an order of magnitude in the topside ionosphere (1000–2500 km) and increase rapidly below 1000 km. This may be an indication that auroral precipitation has a significant effect in the formation and control of the Jovian ionosphere at high latitudes.

As was previously mentioned, the source of energetic particles responsible for the aurora is thought to be the Io plasma torus [*Thorne and Tsurutani*, 1979]. Intense fluxes of charged particles have been detected in the inner magnetosphere of Jupiter by both Voyager spacecrafts [*Bridge et al.*, 1979; *Krimigis et al.*, 1979; *Vogt et al.*, 1979; *Gehrels et al.*, 1981]. Especially intense electron and ion fluxes were detected in the vicinity of the plasma torus. Both the energetic and the thermal ion populations in this torus, and throughout the inner magnetosphere, contain significant fractions of heavier ions such as sulfur, oxygen, and sodium. Various instruments on V1 and V2 [e.g., *Bagenal and Sullivan*, 1981] have determined that the total ion density was as much as 2000 cm^{-3} in the torus.

The plasma wave experiments (PWS) on V1 and V2 revealed a variety of different type waves near the torus, such as whistler mode chorus and hiss as well as electrostatic waves [*Scarf et al.*, 1979; *Gurnett et al.*, 1979; *Kurth et al.*, 1980]. Many of these waves can trigger electron, and possibly ion precipitation, into the atmosphere of Jupiter by means of pitch angle scattering due to wave-particle interactions. *Thorne and Tsurutani* [1979] argued that the generation of broadband whistler mode waves observed by the plasma wave experiments is consistent with a cyclotron resonance mechanism and could be associated with the precipitation of 100-keV to 1-MeV electrons. *Coroniti et al.* [1980] have suggested that the high-frequency banded whistler mode chorus observed by the PWS in the torus could interact resonantly with electrons of a few keV and result in a precipitated flux of about 6 ergs $cm^{-2}s^{-1}$. *Goertz* [1980] proposed that protons rather than electrons are responsible for the observed auroral emissions. *Thorne* [1981*a*,*b*] considered the possibility that the precipitating particles might be heavier ions.

Barbosa et al. [1981] have recently questioned the association of the Jovian auroral zone solely with the Io plasma torus. They report plasma wave observations revealing the presence of an impulsive electrostatic emission localized to the Jovian middle magnetosphere $10 < R < 30$ R_J that is observed on the edges of the plasma sheet. This same plasma mode has been associated with the presence of terrestrial field-aligned currents in the terrestrial magnetosphere. Using terrestrial analogy, they suggest a process of quasi-permanent, global field-aligned currents for acceleration/precipitation of inverted V electrons, concomitant aurora, and energetic (approximately 10 keV) proton deposition in the middle magnetosphere of Jupiter. Clearly there is much work left to be done in order to understand the underlying particle acceleration sources of Jovian aurorae.

The V1 and V2 UVS instruments detected Lyman alpha and H_2 Lyman and Werner band emissions from the equatorial and mid-latitude regions as well as from the auroral regions. There have also been earth orbit observations of Jovian Lyman alpha by the Copernicus and IUE satellites [*Atreya et al.*, 1982]. These emissions are mostly nonauroral in nature. Resonance scattering of solar Lyman alpha can account for the average Lyman alpha emission, but the presence of a pronounced Lyman alpha intensity bulge located near 80 to 100° S III longitude suggests that the global H distribution is not uniform. The precipitation of particles from magnetospheric convection [*Dessler et al.*, 1981] or flux tube interchange [*Hunten and Dessler*, 1977] has been invoked to explain the inferred increase in atomic hydrogen. The apparent lack of a corresponding bulge in the Lyman and Werner emission bands complicates a particle precipitation interpretation of this phenomena. Indeed, the H_2 emissions present some difficulties in any case. It is difficult for solar excitation alone to produce the 2.8 ± 1.0 kR [*Broadfoot et al.*, 1981] Lyman and Werner band intensities observed in the dayside equatorial thermosphere. However, the nightside Lyman alpha intensity is found to be 5% of the dayglow Lyman alpha, and the H_2 bands practically disappear at night [*Broadfoot et al.*, 1979, 1981; *Sandel et al.*, 1979], suggesting a solar control of the dayglow emissions or an extremely asymmetric magnetospheric precipitation source. Indeed this asymmetry persists at Saturn [*Broadfoot et al.*, 1981] where the magnetospheric particle population is quite different, further strengthening the case for solar control. The dayglow emissions may be some combination of both particle and solar resonance processes, possibly a two-stage excitation process of the H_2 bands involving low-energy electrons and solar photons. A review of the literature on observations of the upper atmosphere and ionosphere of Jupiter, including pre-Voyager observations, can be found in *Atreya and Donahue* [1982].

Atreya and Donahue [1979] have also reviewed the large number of theoretical models describing the upper atmosphere and ionosphere of Jupiter. Here we will briefly review only the theoretical literature concerning the effects of Jovian particle precipitation. *Heaps et al.* [1973] calculated the airglow intensities that would result from energetic electron precipitation, and *Heaps* [1976] explored the implications of this precipitation for heating the neutral atmosphere. *Cravens* [1974] considered the effect of precipitating 20-keV electrons on the atmosphere and ionosphere of Jupiter by calculating airglow intensities; ionospheric densities; and neutral, electron, and vibrational temperatures. *Ashihara and Shimizu* [1977] also studied the auroral neutral and ionospheric temperature structure. *Hunten and Dessler* [1977] suggested that the precipitation of soft electrons and ions may be a source of heat. All these pre-Voyager models contained arbitrary assumptions about the particle fluxes and the geographical extent of the precipitation.

Yung et al. [1982] recently used IUE spectra of the aurora between 1200 and 1700 Å and compared them with synthetic H_2 emission spectra. From this comparison

they conclude that the precipitating particles must be electrons between 1 and 30 keV or other energetic particles that penetrate to number densities of 4×10^{10} to 5×10^{13} cm^{-3} in the atmosphere. *Gerard and Singh* [1982] have developed a model of the interaction of an incident electron beam with an H_2 atmosphere to interpret the Voyager observations. They calculated rates of heating, ionization, H_2 dissociation, and airglow emission.

We will present in this paper a comprehensive theoretical model of both the auroral and nonauroral atmosphere and ionosphere of Jupiter and use this model to study particle precipitation effects on the Jovian upper atmosphere, both at mid- and high-latitudes. The sources of energy in the model include extreme ultraviolet radiation (EUV) and energetic electrons. The precipitation of monoenergetic beams of both 1- and 10-keV electrons at high Jovian latitudes are treated in detail, and the effects of higher energy electrons (approximately 125 keV) and soft electrons at mid- and low-latitudes are also considered. The effects of this precipitation such as airglow excitation, ionization, dissociation, and heating are examined. Also included in this work are calculations of the densities of hydrogen, hydrocarbons, and the important ions as well as the temperatures of the neutral, electron, and ion species.

The model will be described in section 2. In section 3 we will discuss how energy is deposited in the atmosphere by solar EUV radiation and by particle precipitation. In section 4 the effects of this energy deposition on the neutral atmosphere will be discussed, and in section 5 the effects of particle precipitation on the ionosphere will be discussed. The main emphasis of this paper is on the aeronomical effects of particle precipitation in the Jovian upper atmosphere.

2. THE MODEL

The model used to study the aeronomical effects of Jovian precipitation processes is derived from a model of the thermosphere and ionosphere of Saturn [*Waite*, 1981]. The ionospheric chemistry is taken from the earlier models of *Atreya and Donahue* [1976], and the hydrocarbon chemistry is essentially that used by *Atreya et al.* [1981]. In this section, we will summarize the main features of this model. A more detailed description of the model can be found in *Waite* [1981].

2.1. Energy Deposition

Solar ultraviolet radiation is the nonauroral source of energy that drives aeronomical processes in the upper atmosphere of Jupiter. We used the solar flux between 100 and 2000 Å in our calculations (for brevity, we refer to this flux as EUV in the rest of the paper although wavelengths higher than EUV wavelengths are also included); the appropriate values of this flux were taken from measurements by *Heroux and Hinteregger* [1978] and scaled for solar maximum conditions appropriate for the time period of the Voyager mission (H. E. Hinteregger, private communication, 1980) and the heliocentric distance of Jupiter. Since we wish to model typical low- to mid-latitude conditions for nonauroral situations, a solar zenith angle of 60° was utilized.

H_2, He, and H can be photoionized by radiation with wavelengths shortward of 804, 504, and 912 Å, respectively. References for photoabsorption, photoionization, and photodissociation cross sections for these and other Jovian species such as CH_4 can be found in *Waite* [1981] or *Atreya et al.* [1981]. In order to calculate secondary ionization, airglow excitation, neutral species heating, dissociation, and ambient electron heating from both photoelectrons and energetic auroral electrons, it is necessary to determine the electron flux as a function of energy, altitude, and direction.

The two-stream method was used in our model for both the photoelectron and energetic electron flux calculations, and it is described in *Nagy and Banks* [1970] and *Banks and Nagy* [1970]. The pitch angle distribution of electrons is approximated by two streams of electrons, one going up and the other going down. We used 0.5 eV wide energy bins below 10 eV gradually increasing to 400 eV wide bins near 10 keV.

Elastic electron impact cross sections for He and H were taken from *Moiseiwitsch* [1962]. Inelastic cross sections for He and H were taken from *Jackman et al.* [1977] and *Olivero et al.* [1973]. The H_2 elastic cross section, the elastic backscatter probability, and the inelastic H_2 backscatter probability were derived from recent differential elastic cross section measurements of *Shyn and Sharp* [1980, 1981]. The backscatter probabilities for energies greater than 1 keV were extrapolated.

The different sets of inelastic electron impact cross sections reported in the literature for H_2 are in reasonably good agreement [*Miles et al.*, 1972; *Cravens*, 1974; *Cravens et al.*, 1975; *Gerhart*, 1975; *Garvey et al.*, 1977; C. H. Jackman, private communication, 1979]. The one cross section for which the reported values differ significantly is that for the excitation of the $C^1\pi_u$ state (upper level of the Werner band system). Since both the $C^1\pi_u$ cross section and the cross section for the excitation of the $B^1\Sigma_u^+$ state (upper level of the Lyman band system) are important for the interpretation of the Voyager UVS observations, they are tabulated in Table 1 for energies of 20 and 100 eV.

Values of the $B^1\Sigma_u^+$ cross section at 100 eV reported in the literature vary from 2.2×10^{-17} cm^2 to 4×10^{-17} cm^2. However, this latter value, given by *Gerhart* [1975], and the cross section reported by *Garvey et al.* [1977] certainly include the contributions of many higher lying singlet states. We used the *Garvey et al.* [1977] cross section set for our general energy loss calculations; i.e., our calculations of electron fluxes. We also used the *Garvey et al.* [1977] $B^1\Sigma_u^+$ cross section for calculating the Lyman band intensities but considered this as including a large part of the cascading contribution to the Lyman bands from higher states.

The available cross sections for the $C^1\pi_u$ state vary from 3.1×10^{-17} cm^2 [*Yung et al.*, 1982] to 6×10^{-17} cm^2 [*Stone and Zipf*, 1972] at 100 eV (see Table 1*a*). The other reported values lie between these two extremes. *Olivero et al.* [1973] and *Heaps et al.* [1973] used the *Stone and Zipf* [1972] values for the $C^1\pi_u$ cross section in their calculations of Jovian dayglow and auroral emissions. Here, we use the *Garvey et al.* [1977] value for the general energy loss calculations but use a smaller cross section for calculating Werner band intensities. The available cross

TABLE 1*a*. Selected Cross Sections At 100 eV

Reference	$B^1\Sigma_u^+$	$C^1\pi_u$	$B^1\Sigma_u^+$ Plus Cascade	$C^1\pi_u$ Plus Cascade	Lyα
Garvey et al. [1977]*	2.97†	3.92	3.79	4.54	...
Gerhard [1975]	4.0	4.50	...	...	...
Miles et al. [1972]	2.2	1.7	...	...	...
Cravens [1974]	2.2	2.4	3.52	2.76	1.56††
Stone and Zipf [1972]	...	6.0||	...	...	...
Yung et al. [1982]	2.8	3.1	3.7	...	1.2ϕ
Srivastava and Jensen [1977]	2.2	...	...	...	...
deHeer and Carriere [1971]	...	...	...	...	...
This paper for airglow	...	3.2	3.79	2.76	...

*Used in this paper for calculation of electron fluxes.

†Should read as 2.97×10^{-17} cm^2; all entries are in units of 10^{-17} cm^2.

††Includes H(2*S*).

ϕIncludes only H(2*p*); 1.92 with H(2*S*) also included.

||The Stone and Zipf total cross section is scaled from the individual band intensities measured by *Stone and Zipf* [1972], using the Franck-Condon factors of *Spindler* [1969*a*,*b*]. For this calculation see *Cravens* [1974].

TABLE 1*b*. Selected Cross Sections At 20 eV

Reference	$B^1\Sigma_u^+$	$C^1\pi_u$	$B^1\Sigma_u^+$ Plus Cascade	$C^1\pi_u$ Plus Cascade
Garvey et al. [1977]*	2.13†	3.12	2.40	3.32
Cravens [1974]	0.9	1.1	1.3	1.2
Stone and Zipf [1972]	...	4.9	...	...
Yung et al. [1982]	1.5 ± 0.5	0.94 ± 0.6	2.15	1.03
Srivastava and Jensen [1977]	1.9 ± 0.6	...	...	...
This paper for airglow	...	...	2.40	1.77

*Used in this paper for calculation of electron fluxes.

†Should read as 2.13×10^{-17} cm^2; all entries are in units of 10^{-17} cm^2.

section values for 20 eV are also listed in Table 1*b*. At this energy, the spread in the given $B^1\Sigma_u^+$ cross section is again less than the ones for the $C^1\pi_u$ state. An energy of 20 eV is only slightly larger than the threshold energies for both the B and C states (11.37 and 12.40 eV, respectively); and, given the cross sections increase rapidly at energies near the threshold, the calculated Lyman and Werner band intensities, due to photoelectron excitation (given in the next section), will have large uncertainties. The cross section used in this paper for the emission of Lyman alpha due to electron impact dissociation of H_2 is also listed in Table 1*b*.

We will calculate only the total integrated band intensities for the Lyman and Werner systems; however, it should be pointed out that these total intensities could be broken down into individual band intensities in the manner described in *Cravens* [1974], *Gerard and Singh* [1982], or *Yung et al.* [1982]. Radiative transfer effects are also not considered for the Lyman and Werner bands, this requires that auroral electrons not be so energetic as to penetrate into the hydrocarbon layer since the hydrocarbons can absorb these emissions or to penetrate to levels where column depths of H_2 exceed 10^{20} cm^{-2} so as to avoid multiple scattering fluorescence effects. *Yung et al.* [1982], using IUE spectra containing H_2 Lyman and Werner band features, have ascertained that in some instances the incident electrons do not penetrate below the hydrocarbon homopause since little extinction is evident in the Lyman and Werner bands. On other occasions more extinction was observed, indicating some penetration into the hydrocarbon layer. Using these results and a radiative transfer model for the resonance scattering of Lyman alpha, *Yung et al.* [1982] deduced that the incident electrons are in the 1- to 30-keV range. Consequently, we are, in most cases, justified in ignoring radiative transfer effects for the H_2 band systems, since the 20% enhancement of the Lyman bands due to reflection of the downgoing flux by Rayleigh scattering of H_2 [*Yung et al.*, 1982] is well within the present cross section uncertainties (Tables 1*a* and 1*b*). Radiative transfer cannot be ignored for Lyman alpha; however, for electrons in the above energy range, we will still be able to estimate the Lyman alpha intensity within a factor of 2 and thus be able to determine if our calculated Lyman alpha intensities are in rough agreement with the Voyager measurements.

Auroral optical emissions of photoelectron dayglow represent only a fraction of the total energy deposited in the Jovian atmosphere by incident auroral electrons or by EUV radiation. Energy can also be deposited as ionization, dissociation, vibrational excitation, neutral heat, and/or electron heat. The rate at which energetic electrons heat the ambient electrons is given by *Swartz et al.* [1971]. The amount of neutral heat and dissociation that results directly from electron impact on H_2 can be calculated in the manner described by *Cravens et al.* [1975]. There are also indirect sources of heat from other processes taking place after the initial excitation of H_2 (or H or He). These will be discussed in the next section.

Two different auroral models are considered, one for a 1-keV (actually 950 eV) monoenergetic beam and one for a 10-keV (actually 9800 eV) monoenergetic beam. The actual spectrum of incident electrons is not known and probably covers a range of energies in a time dependent fashion; however, these two energies should enable us to get a feeling for how the incident energy influences the aeronomical processes associated with the aurora. In section 4, we will also determine some of the effects of the precipitation of 125-keV electrons that penetrate below the homopause, as well as low-energy electrons (20 eV) that deposit their energy above the ionospheric peak at a density level of about 10^8 cm^{-3}.

The depth in the atmosphere to which an incident beam of electrons with a given energy penetrates depends on the characteristics of the neutral atmosphere. We will use a model of the neutral atmosphere resulting from theoretical modeling of the Voyager UVS stellar occultation and solar occultation data analyzed by *Atreya et al.* [1981] and *Festou et al.* [1981]. This analysis yields altitude profiles of composition and temperature and the location of the homopause as well as the eddy diffusion coefficient for low latitudes. Auroral heating and associated thermospheric transport processes will probably alter the neutral atmosphere at high latitudes; however, these changes will mainly affect the adopted atmospheric density/altitude scale used, and the basic conclusions that we will reach in this paper are independent of the detailed atmospheric structure. To a lesser extent, the same thing can be said about proton or heavy ion aurora. The aeronomical effects of auroral precipitation will be similar regardless of the identity of the incident particles as long as those particles reach roughly the same atmospheric level relative to the hydrocarbon homopause. Of course, the energy of the ions would need to be higher for them to reach the same level as electrons; for example, a 1-MeV ion penetrates to about the same level as a 10-keV electron.

2.2. *The Neutral and Ionospheric Model*

A one-dimensional theoretical model is used to study the effects of auroral electron precipitation and solar EUV radiation on the Jovian thermosphere and ionosphere. Standard continuity and momentum (diffusion) equations are solved for all the major neutral species: H_2, He, H, CH_4, C_2H_2, C_2H_4, and C_2H_6. The H_2 density always remains close to the values given in *Atreya et al.* [1981] and *Festou et al.* [1981]. A diffusion equation for H^+ is also solved, and photochemical solutions are obtained for the following short-lived ions: $C_2H_5^+$, CH_5^+, CH_4^+, CH_3^+, CH_2^+, CH^+, He^+, HeH^+, H_2^+, and H_3^+. These neutral and ionospheric components of the model are coupled with the electron and ion energy equations and energy deposition code; all parts of the model are run until a steady state solution is reached. A very detailed description of all aspects of this model is given by *Waite* [1981].

The chemical reactions for the neutral atmosphere are basically the same as in *Strobel* [1969, 1975], although with updated reaction rates and cross sections [*Yung and Strobel*, 1980; *Atreya et al.*, 1981]. A variety of eddy diffusion coefficients were tried and will be discussed in section 4. The chemical reactions listed in *Waite* [1981] or *Atreya and Donahue* [1976] were used in the ionospheric calculations. The most important of these reactions are listed in Table 2.

TABLE 2. Summary Of Important Ionospheric Reactions

Reaction	Rate
(1) (e or $h\nu$) + $H_2 \rightarrow H_2^+ + e$	[*Cook and Metzger*, 1964]
$\rightarrow H + H^+ + e$	[*McElroy*, 1973]
(2) (e or $h\nu$) + $H \rightarrow H^+ + e$	[*Atreya and Donahue*, 1976]
(3) $H_2^+ + H_2 \rightarrow H_3^+ + H$	2×10^{-9} cm^3 s^{-1} [*Theard and Huntress*, 1974]
(4) $H_3^+ + e \rightarrow H_2 + H$	$2.8 \times 10^{-7} (200/T_e)^{0.7}$
$\rightarrow H + H + H$	[*Leu et al.*, 1973]
(5) $H^+ + e \rightarrow H + h\nu$	$6.6 \times 10^{-12} (250/T_e)^{0.7}$ [*Bates and Dalgarno*, 1962]
(6) $H^+ + H_2$ ($v'' \geq 4$) $\rightarrow H_2^+ + H$	estimated

Although 90 to 95% of all ions produced are H_2^+, the H_2^+ density in the Jovian ionsophere is very small because reaction (3) forms H_3^+, which then very rapidly dissociatively recombines (reaction (4)). H^+ is the major ion in the upper ionosphere primarily because it recombines very slowly by radiative recombination (reaction (5)). Under some circumstances, vibrationally excited H_2 might also be a sink for H^+ [*Atreya et al.*, 1979].

2.3. *Temperatures*

Heat conduction equations for ions and electrons are solved to obtain the plasma temperatures. References for the thermal conductivities and the cooling rates can be found in *Waite* [1981]. In particular, the new H_2 vibrational and rotational cooling rates of *Waite and Cravens* [1981] are used. For almost all the cases considered, including the aurora, the electron and ion temperatures we obtained were within a few degrees of the neutral temperature for all altitudes below about 2500 km. This was due to strong ion cooling of H^+ by H and the high auroral plasma densities that were produced. Lower plasma densities due to the loss of H^+ to vibrationally excited H_2 could modify this result. We have shown that significant magnetospheric heat fluxes and/or significant amounts of Joule heating can increase the electron and ion temperatures, but these will not be discussed here.

The neutral temperature profile for our model is taken from *Atreya et al.* [1981] and *Festou et al.* [1981] and is assumed to be the same for all our calculations. We are, however, interested in the neutral temperatures that would result from the heating rates we calculate for both the auroral and nonauroral thermosphere. Therefore, we calculate the neutral temperature independently of the rest of the model by using a heat conduction equation. Dynamics will certainly play a role in determining the neutral temperature because the intense heating associated with auroral precipitation at high latitudes will generate strong thermospheric winds. However, the dynamics of the Jovian thermosphere is not well understood; thus, conduction will be the sole means of heat transport considered. The heat conduction equations are:

$$\frac{d}{dz}\left(-\Gamma_n \frac{dT_n}{dz}\right) = Q_n - L_n \qquad (1)$$

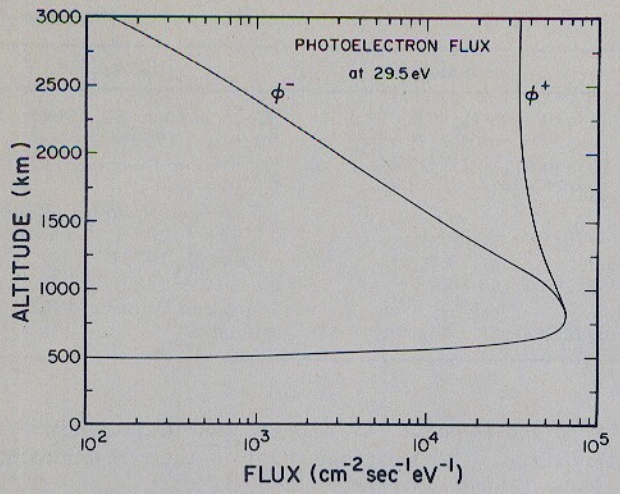

Fig. 1. Calculated photoelectron flux as a function of altitude for an energy of 29.5 eV.

$$\Gamma_n = AT_n^s \qquad (2)$$

where Γ_n is the H_2 thermal conductivity, A is 252 ergs cm^{-1} s^{-1} K^{-1}, and s = 0.751 [*Hanley et al.*, 1970]. Q_n and L_n are the neutral heating and cooling terms, respectively.

The cooling is via infrared radiation by CH_4 and C_2H_2 as described in *Strobel and Smith* [1973]. We used the hydrocarbon profiles deduced by *Atreya et al.* [1981] from the Voyager observations and extended the altitude range of these profiles in a manner consistent with our theoretical hydrocarbon calculations. The sources of heat are solar EUV radiation and energetic electron precipitation. Neutral heating efficiencies are discussed in the next section.

3. Energy Deposition

In this section, we will discuss how energy is deposited into the atmosphere by solar EUV radiation and by auroral electron precipitation. First, we will discuss the photoelectron fluxes calculated by using the two-stream method.

The calculated photoelectron flux as a function of altitude is shown in Figure 1 for an energy of 29.5 eV. These 29.5 eV results show many of the features found at all photoelectron energies and may be taken as typical. The up and down fluxes are almost equal for altitudes below 1000 km, indicating that below this altitude, photoelectron transport is not important and local equilibrium conditions prevail. Above 1000 km, the down flux rapidly decreases, but the up flux decreases only slightly before leveling off at high altitudes. The value at which the up flux levels off is the escape flux (at 29.5 eV). Photoelectrons interact with the ambient electrons more strongly at lower energies, so that at energies lower than 29.5 eV the escape flux will be lower than one might otherwise expect. The photoelectron escape flux as a function of energy is shown in Figure 2.

Calculations of auroral electron fluxes are presented for two cases, categorized either as 'converged' or 'unconverged.' Initially, beams of 1- and 10-keV electrons (actually 950 and 9800 eV, respectively) with 10 ergs

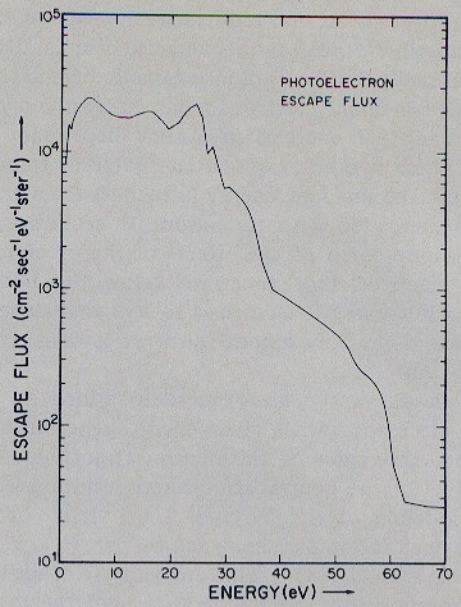

Fig. 2. Calculated photoelectron escape flux as a function of energy.

cm^{-2} s^{-1} were injected into an atmosphere whose H density and electron density were determined solely by EUV conditions (Figures 14 and 17, respectively). These results are denoted 'unconverged.' However, since the auroral precipitation will obviously modify the H and n_e distributions, the auroral fluxes are also calculated by using the new atmosphere. This whole process was iterated until the results converged. We also present auroral fluxes for these 'converged' cases. The 'converged' H and n_e distributions are discussed in the next section; both the calculated n_e and H density are much larger for the aurora than for the absorption of solar EUV only. By presenting both the unconverged and converged electron precipitation cases, we can bracket the possible aeronomical effects due to precipitation. The unconverged case illustrates electron energy deposition in an atmosphere previously controlled by EUV processes. On the other hand, the converged case

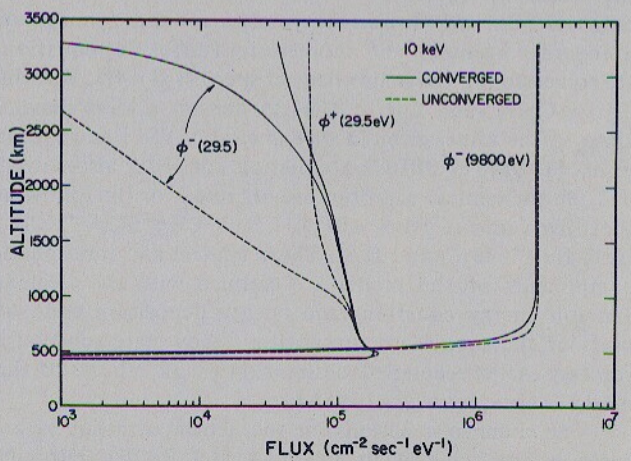

Fig. 3. The '10' keV aurora electron flux as a function of altitude for energies of 9800 and 29.5 eV. The upward electron flux is denoted by the plus and the downward flux is denoted by the minus. Both the unconverged and converged cases are shown for 10-keV monoenergetic electron precipitation.

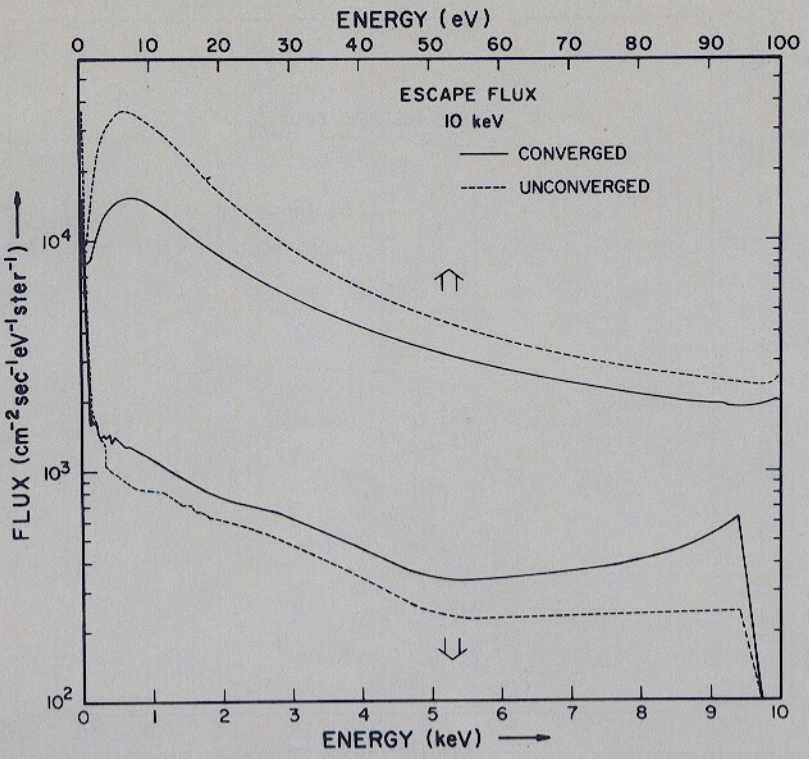

Fig. 4. Escape flux for the 10-keV electron precipitation case as a function of energy. The solid lines show the results for the converged auroral atmosphere case and the dashed lines for the unconverged equatorial atmosphere case. Note the two energy scales, the upper scale for 0 to 100-eV electrons and the lower scale for the overall energy range 0–10 keV.

shows the effect of precipitation on an atmosphere which has been locally confined and acted on by electron precipitation processes until a steady-state 'auroral' atmosphere is produced. The real case that is shaped by both spatial and temporal variations in precipitation and atmospheric transport processes lies somewhere between these two extreme cases.

For the 10-keV aurora we show the flux for the initial energy and for an energy representative of secondary electrons, 29.5 eV (Figure 3). The up flux at 10 keV is negligible (and is off the scale) since the elastic backscatte. efficiency at this energy is extremely small. The down flux at 10 keV begins to fall off at about 750 and 800 km for the unconverged and converged atmospheres, respectively. The primary beam degrades to lower and lower energies (not shown) until the beam finally stops at an altitude of about 450 km. The fluxes at 29.5 eV for the converged and unconverged cases are similar in the vicinity of 500 km. However, for the converged case local equilibrium holds up to about 2000 km; whereas, for the unconverged case, it only holds up to about 1000 km. Notice that at 29.5 eV the escape flux for the converged atmosphere is smaller than for the unconverged atmosphere.

The escape flux as a function of energy is shown in Figure 4 for the 10-keV aurora and in Figure 5 for the 1-keV aurora. Escaping secondary electrons account for most of the escape flux for energies less than about 200 eV and backscattered primary electrons for energies greater than 200 eV. Only a small sample of the calculated photoelectron and auroral fluxes are presented in the figures. Volume emission rates, ionization rates, heating rates, and H_2 dissociation rates were calculated by using the complete set of electron fluxes at all energies and the appropriate altitude.

The volume emission rate is shown for the sum of all the Lyman bands and includes the continuum accounting for about 25% of the total (Figure 6). These results are for the 1- and 10-keV aurora in the converged atmosphere. The altitudes of peak energy deposition for both aurora lie above the hydrocarbon layer; the Voyager UVS measurements give this layer at around 350 to 400 km in the equatorial region [*Atreya et al.*, 1981; *Festou et al.*, 1981].

The general shapes of the H_2^+ production rate profiles (Figure 7) look the same as the volume emission rate profiles, which is not surprising, since in both cases the energy deposition is into H_2 and the threshold energies are similar. The converged and unconverged profiles look almost the same for 10-keV electrons; but, for 1-keV electrons, the H_2^+ production for the converged atmosphere is smaller; because, in this case, a large amount of the energy is being deposited into H rather than H_2. The total EUV H_2^+ production rate, as well as the photoelectron contribution alone, is also shown in Figure 7.

Except for the 1-keV aurora in the converged atmosphere, H_2^+ production in general accounts for a much larger proportion of the energy deposition than does H^+ production. However, chemical considerations indicate that H^+ is the major ion in the topside Jovian ionosphere. Therefore, a set of H^+ production rate profiles is also presented. Direct ionization of H is less important than dissociative ionization of H_2 as a source of H^+ for the 10-keV aurora in the unconverged atmosphere. For the converged atmosphere, however, the opposite is true (Figure 8). This is due to the greater amounts of atomic hydrogen in the

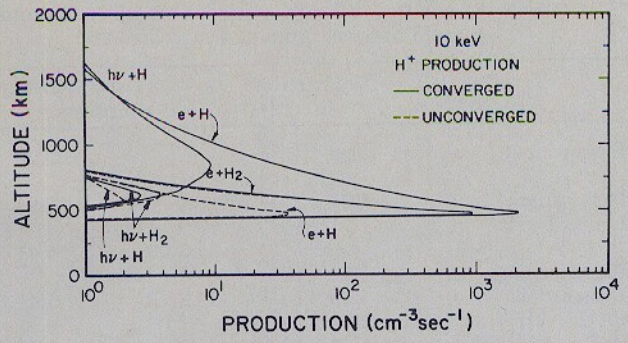

Fig. 8. H^+ production rates as a function of altitude for the 10-keV auroral cases. Note the dramatic increase in the e + H process in the converged (solid line) versus the unconverged (dashed line) auroral atmospheres.

the cross section we used includes it. The total Lyman and Werner band intensity is 235 R. We used a solar flux that was diurnally averaged and a solar zenith angle of 60°; consequently, the subsolar intensity of the total Lyman and Werner bands is 940 R. These integrated band intensities are a factor of 3 smaller than the intensity observed by the Voyager UVS experiment on the dayside [*Broadfoot et al.*, 1979, 1981] and might indicate that some diffuse particle precipitation is required at low latitudes [*Broadfoot et al.*, 1981]. It is also possible that the discrepancy may be due to errors in the cross sections at photoelectron energies (see section 2).

Table 4*b* includes the energy deposition by excitation of the lowest vibrational levels of H_2 by direct electron impact. The vibrational levels, especially the higher ones, can also be populated by cascading from higher lying electronic levels, in particular the $B^1\Sigma_u^+$ and $C^1\pi_u$ states. The column production of H_2 vibrational quanta in the ground state can be calculated [*Cravens*, 1974] by using the excitation rates of the B and C states, together with Franck-Condon factors [*Spindler*, 1969*a*, *b*].

Table 3*b* also includes the sum of the contributions from several processes that lead directly to H production and to heating. The most important of these processes is excitation to the $b^3\Sigma_u^+$ state. The individual contributions of different processes to H production or heat are not indicated in Table 3*b* but are described in *Cravens* [1974] and *Cravens et al.* [1975].

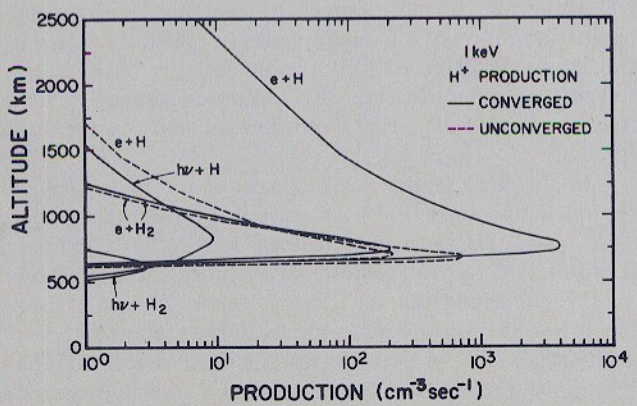

Fig. 9. H^+ ion production as a function of altitude for the 1-keV auroral case. Note the increase in the e + H process in the converged auroral atmosphere.

TABLE 3*a*. EUV Processes: Photons (Primary Processes)

	Column Production, $cm^{-2}\ s^{-1}$	Column Energy Efficiency, %
Total solar energy absorbed for altitudes greater than 400 km	3.80×10^{10} eV	100.00
H_2^+ production	7.41×10^8	31.20
H^+ (from H_2)	8.09×10^7	4.36
H^+ (from H)	6.88×10^7	2.46
He^+	3.50×10^6	0.23
H production	4.19×10^8	2.47
Neutral heat (direct)	$\sim 3.44 \times 10^8$ eV	0.91
Photoelectrons	1.80×10^{10} eV	47.37
Other (airglow, error, etc.)	...	10.98
		100.00

In Table 3*c*, the total EUV column heating rate and H production rate are presented. These totals include other sources of heat and H production; for example, the energy that goes into heating the ambient electrons eventually becomes neutral heat, since the ambient electrons ultimately transfer their energy to the neutral gas. Also, except at very high altitudes, vibrational energy will become neutral heat. Some of the energy stored in H_2^+ eventually becomes heat, although a portion of the energy also goes into dissociation. On the other hand, the energy put into H^+ is not available for heating, since H^+ recombines radiatively unless charge exchange with H_2 ($V \geq 4$) occurs. Exactly how the energy originally deposited via ionization of H_2^+ becomes either heat or energy for H production depends on the details of the ion chemistry. For the purposes of these energy deposition tables, we assume that reaction (3) of Table 2 is always followed by

TABLE 3*b*. EUV Processes: Photoelectrons (Secondary Processes)

	Column Production, $cm^{-2}\ s^{-1}$		Column Energy Efficiency, %
Total photoelectron energy	1.80×10^{10} eV		100.0
Escape to space	3.16×10^7 eV		0.18
Lyman bands	1.35×10^8	7.28	12.93
	235 R*		
Werner bands	1.00×10^8	5.65	
Lyman alpha	2.62×10^7	26.2 R	1.51
H^+ (from H_2)	4.72×10^6		0.54
H^+ (from H)	4.17×10^6		0.31
H_2^+	2.42×10^8		21.87
Vibration (direct)	3.42×10^9		10.26
Vibration (cascade)	1.04×10^9		2.92
H production (direct)	9.36×10^8		11.86
Electron heating	3.01×10^9 eV		16.72
Neutral heating (direct)	3.17×10^9 eV		17.61
He^+	1.70×10^4		0.003
Miscellaneous (H, He, Rydberg, error, ...)	...		3.29
			100.00

*At 60° zenith angle and diurnally averaged. Subsolar intensity would be 940 R plus any resonance scattering.

Total neutral heating efficiency for photoelectrons is 63.00%. Total energy efficiency for H production is 17.88% (including contributions from H_2^+). Mean energy loss per ion pair, W = 72.95 eV/i.p. Mean energy of a photoelectron is 20.2 eV.

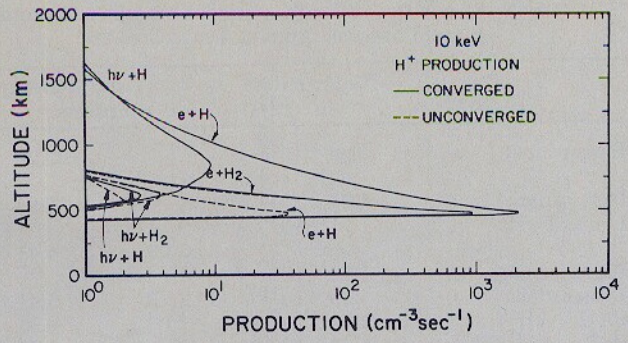

Fig. 8. H^+ production rates as a function of altitude for the 10-keV auroral cases. Note the dramatic increase in the e + H process in the converged (solid line) versus the unconverged (dashed line) auroral atmospheres.

the cross section we used includes it. The total Lyman and Werner band intensity is 235 R. We used a solar flux that was diurnally averaged and a solar zenith angle of 60°; consequently, the subsolar intensity of the total Lyman and Werner bands is 940 R. These integrated band intensities are a factor of 3 smaller than the intensity observed by the Voyager UVS experiment on the dayside [*Broadfoot et al.*, 1979, 1981] and might indicate that some diffuse particle precipitation is required at low latitudes [*Broadfoot et al.*, 1981]. It is also possible that the discrepancy may be due to errors in the cross sections at photoelectron energies (see section 2).

Table 4*b* includes the energy deposition by excitation of the lowest vibrational levels of H_2 by direct electron impact. The vibrational levels, especially the higher ones, can also be populated by cascading from higher lying electronic levels, in particular the $B^1\Sigma_u^+$ and $C^1\pi_u$ states. The column production of H_2 vibrational quanta in the ground state can be calculated [*Cravens*, 1974] by using the excitation rates of the B and C states, together with Franck-Condon factors [*Spindler*, 1969*a*, *b*].

Table 3*b* also includes the sum of the contributions from several processes that lead directly to H production and to heating. The most important of these processes is excitation to the $b^3\Sigma_u^+$ state. The individual contributions of different processes to H production or heat are not indicated in Table 3*b* but are described in *Cravens* [1974] and *Cravens et al.* [1975].

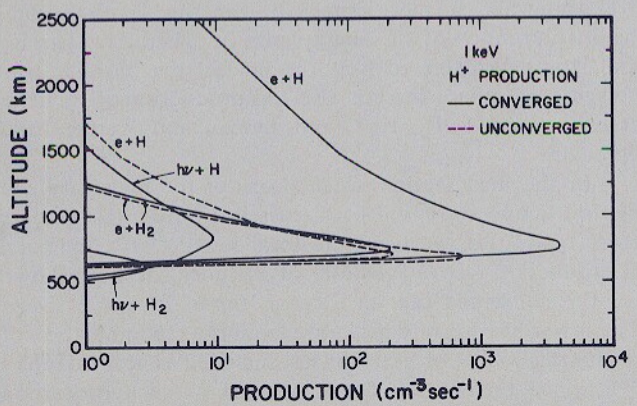

Fig. 9. H^+ ion production as a function of altitude for the 1-keV auroral case. Note the increase in the e + H process in the converged auroral atmosphere.

TABLE 3*a*. EUV Processes: Photons (Primary Processes)

	Column Production, $cm^{-2}\ s^{-1}$	Column Energy Efficiency, %
Total solar energy absorbed for altitudes greater than 400 km	3.80×10^{10} eV	100.00
H_2^+ production	7.41×10^8	31.20
H^+ (from H_2)	8.09×10^7	4.36
H^+ (from H)	6.88×10^7	2.46
He^+	3.50×10^6	0.23
H production	4.19×10^8	2.47
Neutral heat (direct)	$\sim 3.44 \times 10^8$ eV	0.91
Photoelectrons	1.80×10^{10} eV	47.37
Other (airglow, error, etc.)	...	10.98
		100.00

In Table 3*c*, the total EUV column heating rate and H production rate are presented. These totals include other sources of heat and H production; for example, the energy that goes into heating the ambient electrons eventually becomes neutral heat, since the ambient electrons ultimately transfer their energy to the neutral gas. Also, except at very high altitudes, vibrational energy will become neutral heat. Some of the energy stored in H_2^+ eventually becomes heat, although a portion of the energy also goes into dissociation. On the other hand, the energy put into H^+ is not available for heating, since H^+ recombines radiatively unless charge exchange with H_2 ($V \geq 4$) occurs. Exactly how the energy originally deposited via ionization of H_2^+ becomes either heat or energy for H production depends on the details of the ion chemistry. For the purposes of these energy deposition tables, we assume that reaction (3) of Table 2 is always followed by

TABLE 3*b*. EUV Processes: Photoelectrons (Secondary Processes)

	Column Production, $cm^{-2}\ s^{-1}$		Column Energy Efficiency, %
Total photoelectron energy	1.80×10^{10} eV		100.0
Escape to space	3.16×10^7 eV		0.18
Lyman bands	1.35×10^8	7.28	12.93
	235 R*		
Werner bands	1.00×10^8	5.65	
Lyman alpha	2.62×10^7	26.2 R	1.51
H^+ (from H_2)	4.72×10^6		0.54
H^+ (from H)	4.17×10^6		0.31
H_2^+	2.42×10^8		21.87
Vibration (direct)	3.42×10^9		10.26
Vibration (cascade)	1.04×10^9		2.92
H production (direct)	9.36×10^8		11.86
Electron heating	3.01×10^9 eV		16.72
Neutral heating (direct)	3.17×10^9 eV		17.61
He^+	1.70×10^4		0.003
Miscellaneous (H, He, Rydberg, error, ...)	...		3.29
			100.00

*At 60° zenith angle and diurnally averaged. Subsolar intensity would be 940 R plus any resonance scattering.

Total neutral heating efficiency for photoelectrons is 63.00%. Total energy efficiency for H production is 17.88% (including contributions from H_2^+). Mean energy loss per ion pair, W = 72.95 eV/i.p. Mean energy of a photoelectron is 20.2 eV.

TABLE 3c. EUV Processes: Total (Primary Plus Secondary Production Rates)

	Column Production cm^{-2} s^{-1}		Column Energy Efficiency, %
H^+	1.59×10^8		7.53
H_2^+	9.84×10^8		41.43
H production (direct)	1.37×10^9		8.12
Neutral heat (direct)	3.52×10^9 eV		
Electron heat	3.01×10^9 eV	8.90×10^9 eV	23.42
Vibrational energy	2.37×10^9 eV		
Other (airglow, etc.)	...		19.50
			100.00
Neutral heat (direct + electron + vibration)	8.90×10^9 eV	23.42	53.15%
Chemical heat (H_2^+)	1.13×10^{10} eV	29.74	
Direct H production	1.37×10^9		
		3.34×10^9	19.67%
Chemical Hproduction (H_2^+)	1.97×10^9		

The overall EUV column neutral heating efficiency is 53.15%.

TABLE 4b. Energy Deposition Processes for the 1-keV Electron Beam: Converged Auroral Atmosphere

	Column Rate cm^{-2} s^{-1}		Column Energy Efficiency, %
Energy input	6.25×10^{12} eV (10.0 ergs)		100.00
Backscattered	4.34×10^{11} eV		6.94
Lyman bands	1.91×10^{10}	2.94	
		34.3 kR	5.41
Werner bands	1.52×10^{10}	2.47	
Lyman alpha	3.25×10^{10}	32.5 kR	5.41
H^+ (from H_2)	2.90×10^9		0.95
H_2^+	5.64×10^{10}		14.44
Vibration (direct)	7.25×10^9		0.06
Vibration (cascade)	1.52×10^{11}		1.23
H production (direct)	4.75×10^{10}		1.73
Electron heating	1.13×10^{12} eV		18.08
Neutral heating (direct)	1.80×10^{11} eV		2.88
H^+ (from H)	8.68×10^{10}		18.67
He^+	$\sim 4.00 \times 10^5$		~ 0.0
Miscellaneous (H, He, error, etc.)	...		24.20
			100.00

Total neutral heating efficiency including heat from H_2^+, electron heating, and vibrational energy is 32.65%. Total H production (direct plus chamical) is 1.60×10^{11} (5.84% efficiency). Mean energy loss per ion pair, W = 39.81 eV/i.p.

the first channel of reaction (4). In this case, the amount of heat and dissociation is just what would result from the recombination of H_2^+ itself. However, if the second channel of reaction (4) is a significant fraction of the total, then we have somewhat overestimated the amount of 'chemical' heat and underestimated the amount of 'chemical' H production. The total neutral EUV heating efficiency from Table 3c is 53%.

Tables 4 and 5 list column production rates and column energy efficiencies for the 1- and 10-keV aurorae. The energy input is 10 ergs cm^{-2} s^{-1} for all cases and was chosen so that the total Lyman and Werner band intensities (about 90 kR) would be in general agreement with the intensity measured by the Voyager UVS experiment, at least for the unconverged atmosphere. An energy flux of 10 ergs cm^{-2} s^{-1} spread over a 6000-km wide auroral zone in both hemispheres corresponds to a global power of 1.7×10^{13} W. The vertically integrated Lyman alpha volume emission rate is about 25 kR for both aurorae for the unconverged atmosphere and 35 kR for the converged atmosphere. In order to calculate the Lyman alpha intensity, radiative transfer effects must be considered [*Yung et al.*, 1982]; however, a rough estimate gives between 25 and 50 kR, since the peak altitude of energy deposition lies above both the hydrocarbon layer and the bulk of the atomic hydrogen layer. The UVS measurements on the average yield 60 kR for the auroral Lyman alpha intensity [*Broadfoot et al.*, 1981].

TABLE 4a. Energy Deposition Processes for the 1-keV Electron Beam: Unconverged Equatorial Atmosphere

	Column Rate, cm^{-2} s^{-1}		Column Energy Efficiency, %
Energy input	6.25×10^{12} eV (10.0 ergs)		100.00
Backscattered	2.04×10^{11} eV		3.26
Lyman bands	5.03×10^{10}	7.72	
		90.5 kR	14.26
Werner bands	4.02×10^{10}	6.54	
Lyman alpha	2.42×10^{10}	24.2 kR	4.03
H^+ (from H_2)	7.17×10^9		2.34
H_2^+	1.46×10^{11}		37.38
Vibration (direct)	3.35×10^{11}		2.89
Vibration (cascade)	4.02×10^{11}		3.25
H production (direct)	1.61×10^{11}		5.77
Electron heating	5.14×10^{11} eV		8.22
Neutral heating (direct)	5.88×10^{11} eV		9.41
H^+ (from H)	3.23×10^9		0.70
He^+	4.67×10^6		0.001
Miscellaneous (H, He, error, etc.)	...		8.49
			100.00

Total neutral heating efficiency including chemical heat from H_2^+, electron heating, and vibrational energy is 50.68%. Total H production (direct plus chemical) is 4.53×10^{11} (16.23% efficiency). Mean energy loss per ion pair, W = 38.66 eV/i.p.

Considering together the direct and indirect sources of heat and atomic hydrogen, the total heating rate and H production rate can be calculated. The total neutral heating efficiency for either the 1- or 10-keV aurora is about 52% for the unconverged atmosphere which is almost entirely H_2. The heating efficiencies for the converged atmospheres are somewhat smaller, especially for the 1-keV aurora, because so much of the energy goes into H rather than H_2 and is not available to heat the neutral gas. For the converged atmosphere there is also less production of H, vibrationally excited H_2, H_2^+, and Lyman and Werner band emissions.

In the next section, calculations of the H density and neutral temperature will be discussed. In order to calculate these quantities, we need the total heating rate and total H production rate as functions of altitude. These are shown for the converged case in Figures 10 and 11, respectively. The lower heating rate peaks are from the recombination of H and this source of heat was not included as heat in Tables 3–5, since this heat is deposited within the hydrocarbon radiative cooling layer. Tables 3–5 indicate that the total column H production and column heating rates for the aurorae (4.7×10^{11} H atoms cm^{-2} s^{-1} and 5 ergs $cm^{-2}s^{-1}$)

TABLE 5a. Energy Deposition Processes for the 10-keV Electron Beam: Unconverged Equatorial Atmosphere

	Column Rate cm^{-2} s^{-1}		Column Energy Efficiency, %
Energy input	6.25 x 10^{12} eV (10.0 ergs)		100.00
Backscattered	4.85 x 10^{10} eV		0.78
Lyman bands	5.14 x 10^{10}	7.89	14.54
		92.3 kR	
Werner bands	4.09 x 10^{10}	6.65	
Lyman alpha	2.54 x 10^{10}	25.4 kR	4.23
H$^+$ (from H$_2$)	6.26 x 10^9		2.05
H_2^+	1.52 x 10^{11}		38.91
Vibration (direct)	9.62 x 10^{11}		8.31
Vibration (cascade)	4.10 x 10^{11}		3.32
H production (direct)	1.67 x 10^{11}		6.09
Electron heating	1.03 x 10^{11} eV		1.65
Neutral heating (direct)	6.91 x 10^{11} eV		11.06
H$^+$ (from H)	3.45 x 10^8		0.74
He$^+$	~1.30 x 10^8		~0.07
Miscellaneous (H, He, error, etc.)	...		8.32
			100.00

Total neutral heating efficiency including heat from H_2^+, electron heating, and vibrational energy is 52.38%. Total H production (direct plus chemical) is 4.71 x 10^{11} (16.88% efficiency). Mean energy loss per ion pair, W = 39.38 eV/i.p.

are over 2 orders of magnitude larger than what are generated by the absorption of solar EUV radiation alone (3.3 x 10^9 H atoms cm^{-2} s^{-1} and 0.03 ergs cm^{-2} s^{-1}). These auroral production rates are probably diluted by the horizontal transport of H and heat out of the auroral regions by thermospheric circulation. By making the extreme assumption that the auroral H production rate and heating rates are spread uniformly over the whole surface of Jupiter, one can derive globally averaged values of 1.7 x 10^{10} H atoms cm^{-2} s^{-1} and 0.18 ergs cm^{-2} s^{-1}, values which are still considerably larger than the EUV values. It is clear from this that the Jovian aurora must play a central role in both the global energy and atomic hydrogen budget. Low-energy precipitation at mid- and low-latitudes may also be important.

4. Neutral Atmosphere Effects

The aeronomical effects of Jovian particle precipitation can be divided into two categories: the effect of particle precipitation on the neutral atmosphere and on the ionosphere. The neutral atmosphere effects will be discussed in this section, and the ionospheric effects will be discussed in section 5.

4.1. Neutral Composition

Atomic hydrogen is the most important species, other than H_2, in the upper atmosphere of Jupiter. Direct dissociation of H_2 as well as ionization of H_2 and He from solar EUV or particle impact can contribute to the production of H. Each H_2^+ ion produced results in the production of two, three, or four atoms of hydrogen, depending on whether they react with H or H_2 and depending on the branching ratio of the dissociative recombination of H_3^+ (see Table 3). The H_2 + H branch is currently favored (R. Johnson, private communication, 1980), but the branching ratio has never been properly measured. If the H_3^+ ion is vibrationally excited as a result of nonthermal processes such as electron precipitation, the balance could possibly shift toward the H + H + H path. In this model we have assumed that all H_3^+ ions form H_2 and H, but results by *Waite* [1981] indicate that if 30% of the H_3^+ ions follow the H, H, H pathway, the column density of atomic hydrogen that is calculated increases by approximately 20%.

The H^+ ions produced by ionization of atomic hydrogen or dissociative ionization of H_2 ultimately become atomic hydrogen through radiative recombination in the topside ionosphere, three-body association with H_2 in the lower ionosphere, or possibly from a charge exchange reaction with vibrationally excited H_2 ($V \geq 4$) molecules. Indeed H^+ ions could result in a net production of atomic hydrogen if the H_3^+ ions formed in the three-body association and charge exchange reactions recombined with electrons by way of the H, H, H pathway. The He^+ ions formed in the ionosphere by EUV or particle processes can also produce H by reaction with H_2; however, they are a small source of H due to the falloff of He with respect to H_2 above the homopause.

In addition to ionization processes, dissociation of H_2 by photons and electrons also produces H. For solar EUV processes, 8% of the total column-integrated EUV energy absorbed above 400 km goes into production of H by direct dissociation; and, for electron precipitation, approximately 6% of the total energy results in direct dissociation. Including the ionospheric sources of H increases the efficiencies for H production to about 20% for solar EUV and about 17% for electron precipitation (see Tables 3–5). Total H production rates versus altitude are shown in Figure 11.

The loss of atomic hydrogen proceeds by three-body recombination reactions with either H, C_2H_2, or CH_3. The pressure dependence of these reactions confines the main loss of H to the well-mixed, lower atmosphere near a density level of 1.5 x 10^{13} cm^{-3}. Thus, production of atomic hydrogen takes place mostly in the ionosphere near

TABLE 5b. Energy Deposition Processes for the 10-keV Electron Beam: Converged Auroral Atmosphere

	Column Rate cm^{-2} s^{-1}		Column Energy Efficiency, %
Energy input	6.25 x 10^{12} eV (10.0 ergs)		100.00
Backscattered	7.80 x 10^{10} eV		1.25
Lyman bands	4.52 x 10^{10}	6.94	12.80
		81.2 kR	
Werner bands	3.60 x 10^{10}	5.86	
Lyman alpha	2.76 x 10^{10}	27.6 kR	4.59
H$^+$ (from H$_2$)	5.56 x 10^9		1.82
H_2^+	1.34 x 10^{11}		34.30
Vibration (direct)	5.97 x 10^{11}		5.16
Vibration (cascade)	3.60 x 10^{11}		2.92
H production (direct)	1.42 x 10^{11}		5.18
Electron heating	2.87 x 10^{11} eV		4.59
Neutral heating (direct)	5.43 x 10^{11}		8.69
H$^+$ (from H)	1.78 x 10^{10}		3.83
He$^+$	~1.20 x 10^8		~0.06
Miscellaneous (H, He, error, etc.)	...		14.81
			100.00

Total neutral heating efficiency is 46.06%. Total H production is 4.10 x 10^{11} (14.69% efficiency). W = 39.22 eV/i.p.

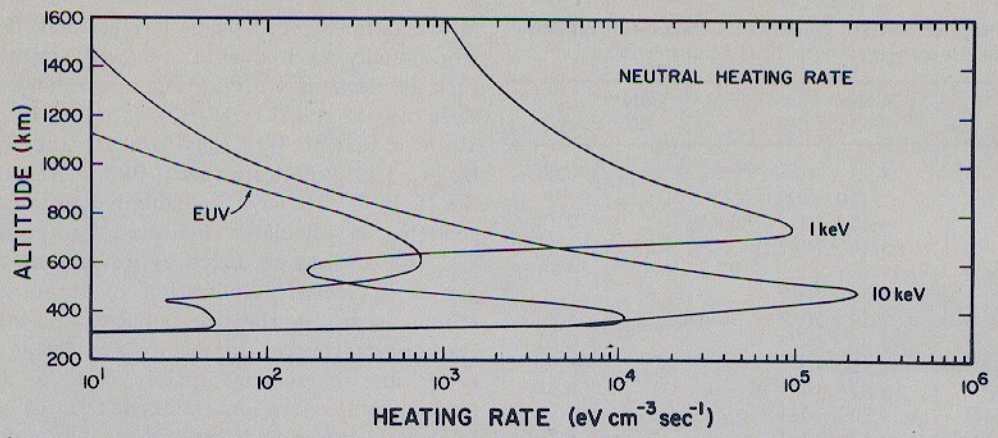

Fig. 10. The neutral heating rate as a function of altitude for the 1- and 10-keV electron precipitation cases in the converged auroral atmosphere and for solar EUV processes.

a density level of 8×10^{10} cm^{-3}, and then the H is transported downward into the homosphere where it recombines. If the ratio of C_2H_2 to H is less than approximately 5×10^{-3} and the ratio of CH_3 to H is less than approximately 2×10^{-4}, three-body recombination of atomic hydrogen with itself is the dominant loss process. The potential importance of the hydrocarbon molecules in the atomic hydrogen loss process makes it necessary to determine their density distributions as realistically as possible. We have chosen the lower-boundary values of C_2H_2, C_2H_6, and CH_4 so that they match the equatorial mixing ratios in the lower atmosphere inferred by the Voyager IRIS experiment [*Hanel et al.*, 1979]; we then adjusted the eddy diffusion coefficient so as to obtain best agreement with the densities of CH_4, C_2H_2, and C_2H_6 inferred from Voyager UVS measurements near the homopause [*Atreya et al.*, 1981]. A reasonable fit to the measured hydrocarbons (Figure 12) is obtained with an eddy diffusion coefficient that varies as the inverse of the square root of the atmospheric density $K \propto 1/\sqrt{M}$ and reaches a value of $K_h = 9 \times 10^5$ cm^2 s^{-1} at the homopause (350 km) [*Atreya et al.*, 1981]. An exact determination of the hydrocarbon densities is not the main purpose of this paper (see *Yung and Strobel* [1980]). However, the present values of the model are adequate to calculate the first order effects of loss of H through reaction with hydrocarbon species.

The loss of H is dominated by C_2H_2 below 375 km and by reaction with itself above that altitude. Hydrocarbon reactions dominate the loss of H at altitudes below the hydrocarbon homopause for larger values of the eddy diffusion coefficient ($K_h = 7 \times 10^7$ cm^2 s^1). This increased loss rate plus more rapid downward transport of H results in a peak H density for the large K_h case that is a factor of 10 smaller than for the nominal case ($K_h = 9 \times 10^5$ cm^2 s^{-1}). For smaller values of K_h (approximately 10^4 cm^2 s^{-1}), molecular diffusion dominates the transport of H, and the loss of atomic hydrogen by reaction with itself is the more important loss process in the region of the H peak. However, the peak density of H increases only 40% above that of the nominal case. This indicates that in the nominal case a factor of 2.5 reduction in the C_2H_2 will result in a 20% increase in the peak H density.

Relationships between the planetary Lyman alpha albedo and the eddy diffusion coefficient for solar EUV processes can be derived by using our calculated column H abundance above the CH_4 absorption layer or CH_4 homopause for a range of values of K_h (see Figure 13). These column abundance values for H can be combined with the calculations of *Clarke et al.* [1980] to obtain a relationship between K_h and the planetary Lyman alpha albedo (Figure

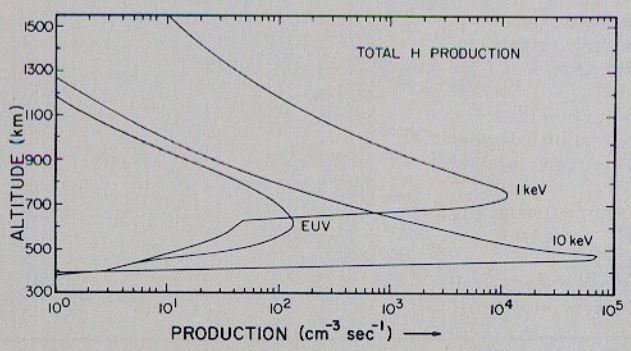

Fig. 11. The total H production rates as a function of altitude for the 1- and 10-keV auroral cases and for EUV processes.

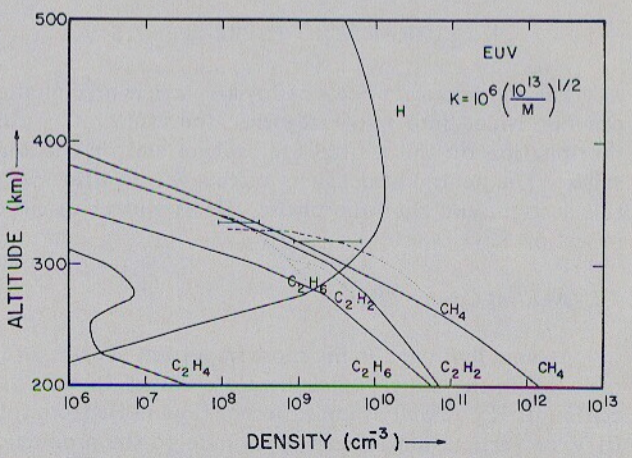

Fig. 12. Hydrocarbon density profiles as a function of altitude for an eddy diffusion coefficient that varies as the $1/\sqrt{M}$, where M is the atmospheric density and reaches a value of 9.5×10^5 cm^{2}s^{-1} at the methane homopause. The solid line denotes the model density profiles referred to as the nominal model, and the dotted lines show the CH_4, C_2H_2, and C_2H_6 derived from Voyager 2 EUVS stellar occultation measurements [*Atreya et al.*, 1981].

13). This relationship includes the effects of solar maximum EUV fluxes and of suitably high thermospheric temperatures, appropriate for the Voyager encounter.

4.2. *Auroral Atomic Hydrogen*

First, we will consider the atomic hydrogen distribution resulting from the 1- and 10-keV aurora themselves, and we will then discuss the possible effects of the high-latitude auroral H production in the low- and mid-latitude thermosphere. We have calculated the atomic hydrogen distribution, hydrocarbon distributions, and neutral temperature profile in the aurorae assuming no horizontal H dispersion. We have assumed that the standard hydrocarbon photochemical scheme we have used is not grossly modified by auroral processes, although a change in hydrocarbon mixing ratios in the high-latitude auroral atmosphere has been inferred from Voyager IRIS measurements [*Hanel et al.*, 1979]. Changes in the hydrocarbon mixing ratios in the auroral case for moderate values of K_h have little effect on the auroral atomic hydrogen profiles, since the increased H concentrations make the H + H + H_2 the most important auroral loss process for H. We have also ignored, for the present, effects of horizontal transport of atomic hydrogen by thermospheric winds. The atomic hydrogen profiles that result from electron precipitation within these constraints are shown in Figure 14, along with the nominal EUV produced atomic hydrogen profile. The eddy diffusion coefficient was a constant 2 x 10^5 cm^2 s^{-1}, although we also tried K_h = 2 x 10^6 cm^2 s^{-1} for the 10-keV aurora and found auroral H to be quite insensitive to K values in that range. Unfortunately, the auroral eddy diffusion coefficient is an unknown quantity. The peak concentration in all three cases lies at an altitude of approximately 400 km, very near the level of the methane homopause. The H peak density for EUV processes is 1.3 x 10^{10} cm^{-3} and results in a column-integrated H density above the methane absorbing layer of 1.75 x 10^{17} cm^{-2} (see Figure 13). For the 1-keV electron beam with a total energy flux of 10 ergs cm^{-2} s^{-1}, the peak density is 2.0 x 10^{11} cm^{-3} with a corresponding column depth of 3.69 x 10^{18} cm^{-2} s^{-1}, and for the 10-keV case with an energy flux of 10 ergs cm^{-2} s^{-1}, the peak density is 4.2 x 10^{11} cm^{-2} and a column depth of 7.16 x 10^{18} cm^{-2} (Figures 13–14).

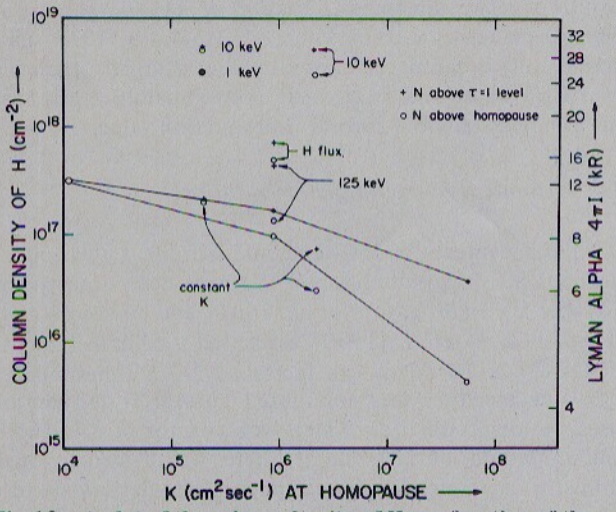

Fig. 13. A plot of the column density of H as a function of the eddy diffusion coefficient (K) at the methane homopause. The right-hand ordinate scale gives the resonance-scattered planetary Lyman alpha contribution that corresponds to the column density of H on the left-hand ordinate. These Lyman alpha results are taken from *Clarke et al.* [1981]. Two values for the column density of H are given for each calculation, the one denoted by a + sign gives the column depth of H above a level where hydrocarbon optical depth at Lyman alpha equals unity, and the one denoted by o gives the H column depth above the mathematically defined methane homopause where the eddy diffusion coefficient for methane equals the Fickian diffusion coefficient. Several cases are shown in the figure. The solid lines connect the solar EUV produced atomic hydrogen results for various eddy diffusion coefficient profiles. Several calculations for the solar EUV case with constant K are also shown. Auroral cases for K = 2 x 10^5 cm^2 s^{-1} are shown for the 1- and 10-keV auroral beams, and there is also a case for the 10-keV electron aurora where K_h = 2 x 10^6 cm^2 s^{-1}. The 125-keV electron precipitation case with K = 9 x 10^5 cm^2 s^{-1} and a globally averaged downward H flux case have also been introduced to illustrate the effects of the aurora on the global H budget.

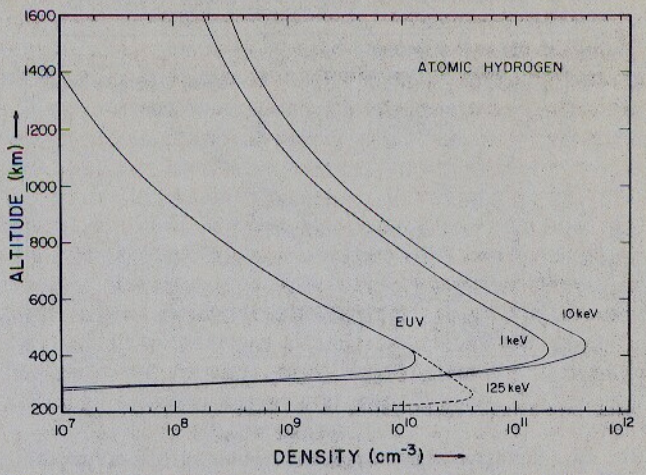

Fig. 14. Model atomic hydrogen profiles as a function of altitude for the solar EUV case and for 1-, 10-, and 125-keV electron precipitation cases where the total energy flux of the precipitating electrons equals 10 ergs cm^{-2} s^{-1}.

Electron precipitation with an incident energy flux of 10 ergs cm^{-2} s^{-1} results in a very large production of atomic hydrogen; although the energy flux of the 10- and 1-keV electron beams are the same, the 10-keV electrons produce more atomic hydrogen (Figures 13–14). The reason for this was alluded to in section 3. A further understanding of this can be obtained by examining the results of *Waite* [1981] for the Saturnian atmosphere with composition and eddy diffusion coefficient similar to those on Jupiter (see Figure 15). The 10-keV beam on Saturn produces H more efficiently than lower energy electron beams at all levels of incident electron energy fluxes, basically because lower energy beams deposit more of their energy at higher altitudes where H rather than H_2 is the major species. The result is less of the beam energy goes into dissociation of H_2 via reaction of H_2^+ with H_2 and subsequent recombination of H_3^+ ions.

The conversion of the upper atmosphere into atomic hydrogen by electron precipitation processes has a pronounced effect on the partitioning of energy among the various processes. The effects in a one-dimensional atmosphere that has reached an equilibrium between H and H_2

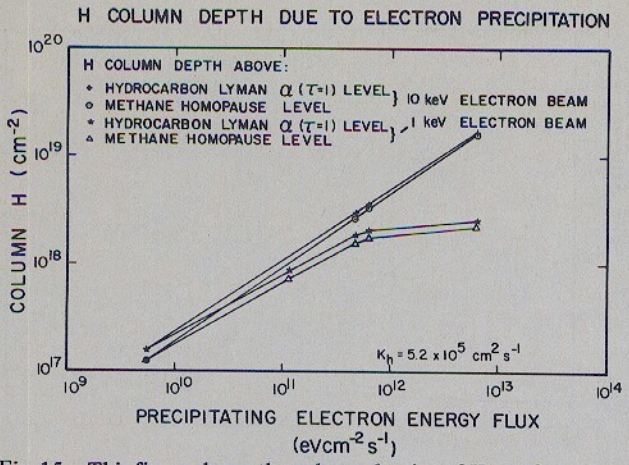

Fig. 15. This figure shows the column density of H as a function of the energy flux of the precipitating electrons for both 1- and 10-keV monoenergetic electron beams. These results are taken from the Saturn calculation of *Waite* [1981] but illustrate the effect of auroral electrons for any H_2 dominated atmosphere.

after the continued deposition of 10 ergs cm^{-2} s^{-1} of electron precipitation were shown in Tables 4–5 for the 1- and 10-keV beam, respectively. The contrast is striking for the 1-keV case (compare Tables 4*a*-4*b*) due to the relatively large H:H_2 ratio (0.02 versus 1.1) present at the level of maximum electron energy deposition (approximately 700 km). The Lyman and Werner band intensities for the converged auroral atmosphere are only 34 kR versus 90 kR for the earlier standard (unconverged) atmosphere model. The Lyman to Werner band emission ratio is still 1.19. The vertically integrated Lyman alpha volume emission rate is increased by a factor of 1.34. The ratio of H_2 band emission to Lyman alpha emission is now 1.06, which is significantly different from the standard atmosphere value of 3.74. H_2^+ production now accounts for only 14% of the column-integrated energy deposition in comparison with the standard atmosphere value of 37%. H^+ production has come up to 20% of the total energy from the earlier value of 3%. The total heating efficiency has decreased from 51 to 33%, and the column H production (direct plus chemical) is down from 16% to only 6%. The mean energy loss per ion pair is up slightly to 39.81 eV/ion pair.

The results for the 10-keV case exhibit similar trends, but are much less pronounced owing to the smaller H:H_2 ratio of both the unconverged atmosphere (2.71×10^{-3}) and the converged auroral atmosphere (0.14) at the level of maximum energy deposition. In the 10-keV case, the H_2 Lyman and Werner band emissions decreased approximately 10% to 81.2 kR, and the integrated Lyman alpha volume emission rate increased slightly to 27.6 kR. The resulting ratio for H_2 band emission to Lyman alpha emission is now 2.94 rather than the previous standard model atmosphere value of 3.63. H_2^+ production efficiency is down slightly to 34%, and H^+ production is up to 4%. The neutral heating efficiency is decreased to 46%, and the H production efficiency is down slightly to 14.7%. The energy loss per ion pair is almost exactly as before, 39.22 eV/ion pair.

These results indicate the importance of knowing the atomic hydrogen altitude distribution in order to interpret properly the Voyager ultraviolet auroral airglow results. Unfortunately, the auroral atomic hydrogen densities that we have calculated (Figure 14) are only upper limits to the true auroral H densities (for incident electron beam energies of 1 and 10 keV), because our calculation only included vertical diffusive transport of H and neglected horizontal transport. Horizontal transport will result from thermospheric winds generated by auroral heating.

We have tried to simulate the potential atmospheric effect at lower latitudes of redistribution of aurorally produced atomic hydrogen by introducing a downward flux of H in the topside ionosphere equal to the integrated auroral H production above the methane homopause and uniformly distributed over the Jovian surface. The result is a factor of 5 increase in our calculated column H over that of the nominal solar EUV model ($K_h = 10^6$ cm^2 s^{-1}) even though the same nominal eddy diffusion coefficient was employed (see Figure 13). The resulting atomic hydrogen profile (not shown, although the column density is shown in Figure 13) for the H down flux case $K_h = 10^6$ cm^2 s^{-1} has a peak density of 4.1×10^{10} cm^{-3} as compared with a peak density of 1.1×10^{10} cm^{-3} for the solar EUV produced profile. Comparison of these atomic hydrogen results (Figure 13) with the inferred column H values of *Clarke et al.* [1980] indicates that there is indeed enough aurorally produced H to explain current observations if aurorally produced H is globally redistributed in the simple fashion we have assumed. *Clarke et al.* [1980] suggest an average planet-wide H column of $3.2–4.4 \times 10^{17}$ cm^{-2} that is only a factor of approximately 2 greater than our solar EUV value and a factor of approximately 2 less than our evenly distributed auroral H production value.

4.3. *Atomic Hydrogen Equatorial Bulge*

Enhancements in low- and mid-latitude Lyman alpha at about 80° longitude (system III) have been observed by Voyager UVS [*Broadfoot et al.*, 1981] and by *Clarke et al.* [1980]. *Clarke et al.* [1980] estimated a column H depth of $1.5–2.1 \times 10^{18}$ cm^{-2}, a factor of 2–3.5 times smaller than our steady state, nondiluted auroral H production cases. A longitudinal asymmetry of a factor of 3 in the H column would be possible if there was a strong longitudinally asymmetric thermospheric circulation pattern driven by a longitudinally asymmetric auroral heating at higher latitudes. The atomic hydrogen produced from precipitation sources might then be redistributed throughout the Jovian thermosphere to produce an asymmetric H bulge at lower latitudes. On the earth, an analogous mechanism is thought to be responsible for latitudinal thermospheric temperature gradients as well as transport of major constituents like O and of aurorally produced minor constituents such as NO to low latitudes in the earth's upper atmosphere [*Cravens et al.*, 1979]. In fact, significant longitudinal asymmetries were observed for NO in the earth's thermosphere [*Cravens and Stewart*, 1978]. Better morphological definition and quantification of the Jovian auroral sources are needed before dynamical calculations can be undertaken to quantify such a scenario.

We have suggested that the longitudinally asymmetric Lyman alpha emissions are produced by redistribution of

auroral H by thermospheric winds. However, others [e.g., *Dessler et al.*, 1981] have attributed this same phenomena to a postulated longitudinally asymmetric particle precipitation at low- and mid-latitudes.

There are two indications in the Voyager UVS data that suggest particle precipitation processes might indeed affect the Jovian equatorial thermosphere. The Lyman and Werner band intensities of 2.8 ± 1.0 kR observed in the dayside equatorial thermosphere [*Broadfoot et al.*, 1981] could possibly imply a total electron precipitation energy flux of 0.3 ergs cm^{-2} s^{-1} over the dayside disc [*Broadfoot et al.*, 1981; *Atreya et al.*, 1981]. The second possible indication of low-latitude precipitation is the longitudinal asymmetry of the planetary Lyman alpha [*Broadfoot et al.*, 1981; *Clarke et al.*, 1980; *Dessler et al.*, 1981]. It has been suggested that the excess intensity of the Lyman alpha bulge reflects an increase in H, which can be attributed to precipitating particles at very high [*Dessler et al.*, 1981] or very low energies [*Sandel et al.*, 1980] that are longitudinally asymmetric as a result of inhomogeneities in the Jovian magnetosphere.

We have looked into both the soft and the hard electron scenarios. To study the effects on the atmospheric composition of an energetic particle beam that deposits its energy below the level of the methane homopause (as suggested by *Dessler et al.* [1981]), we have introduced a production rate of atomic hydrogen equal to that of the 10 ergs cm^{-2} s^{-1} 10-keV monoenergetic electron beam but with the peak production placed at the much lower altitude of 250 km which corresponds to electrons with 125 keV. This procedure should enable us to simulate roughly the effects of a very energetic beam on the atomic hydrogen distribution, because the efficiency for the production of H is about the same for either 10- or 125-keV electrons. Actually, H production efficiency for the 125-keV electrons might be as much as 30% smaller than for the 10-keV electrons, because some of the H_3^+ ions will react with CH_4 rather than electrons. Consequently, these results represent an upper limit for the calculated atomic hydrogen, but this does not change our qualitative conclusions concerning hard electron precipitation. The atomic hydrogen profile that results from this production is shown by the dashed line in Figure 14 along with the EUV and 1- and 10-keV atomic hydrogen profiles. Hydrogen reaches a peak density of 3×10^{10} cm^{-3} at an altitude of 260 km. The peak density is reduced by a factor of 13, compared with the 10-keV auroral case. This reduction is the result of increased losses of atomic hydrogen with itself and hydrocarbons at this greater depth in the atmosphere. The H concentration near the level of the homopause, relative to the solar EUV produced H, is enhanced very little, resulting in almost no increase of the column abundance of H above the methane homopause and only a factor of 2 increase in column abundance above the hydrocarbon Lyman alpha unit optical depth ($\tau = 1$) level. Since most of the beam energy is deposited near the hydrocarbon Lyman alpha $\tau = 2$ level, some Lyman and Werner photons (about 10 to 15 kR) will escape and result in an enhancement in the Lyman and Werner band airglow at the same locations where the Lyman alpha is enhanced. However, no such Lyman and Werner band asymmetry has been reported. More energetic electrons (> 125 keV) will penetrate even deeper, thereby completely shutting off this Lyman and Werner band emission; but, at the same time, any atomic hydrogen that could participate in the solar Lyman alpha resonance scattering will be effectively buried too deep to be observed and will also be chemically destroyed by the hydrocarbons. Thus, energetic particles do not seem to be a satisfactory explanation of the observed Lyman alpha longitudinal bulge that is observed.

The low-energy particle precipitation scenario presented by *Sandel et al.* [1980] may be more likely than the high-energy precipitation scenario. Low-energy electrons with energies near 20 eV deposit their energy near the 10^8 cm^{-3} H_2 level, where the H density is between 2 and 6×10^7 cm^{-3}. The resonance scattered Lyman alpha will be enhanced for a 20-eV beam due to the increased amount of H. Consequently, a longitudinally asymmetric precipitation of 20-eV electrons will produce an H bulge; however, once again the Lyman and Werner band emission will also be asymmetric. When we tried a 20-eV beam with an energy flux of 0.5 ergs cm^{-2} s^{-1}, our calculated electron density also increased by about a factor of 3 (see section 5) as did our neutral heating rates (about 0.2 ergs cm^{-2} s^{-1}). We calculated a neutral exospheric temperature of 1070 K (Figure 16) and plasma temperatures that were significantly greater than the neutral temperature at altitudes above 1850 km. We calculated an electron temperature of 9000 K and an ion temperature of 6500 K at 3300 km.

However, a difficulty with soft electron precipitation which was recognized by *Broadfoot et al.* [1981] is that there is no apparent reason for the soft electron precipitation to shut off at night as would be required in order to explain the day/night asymmetry of the Lyman and Werner band emissions. Therefore, the longitudinal asymmetry in Lyman alpha remains unexplained, although global redistribution of H by meridional winds and soft particle precipitation are reasonable possibilities.

4.4. *Neutral Temperature*

In the auroral zone, the column heating efficiency is approximately 50% (Tables 4–5), and this will be true independent of the identity of the precipitating particles. Therefore, in the case of a 10 ergs cm^{-2} s^{-1} aurora, the column heating rate is about 5 ergs cm^{-2} s^{-1}. As described in section 2, the neutral heating rates for the converged auroral atmosphere are shown in Figure 10. The exospheric temperatures obtained are only 260 K for solar EUV heating alone, 1900 K for the 10-keV aurora, and 3000 K for the 1-keV aurora (Figure 16). The temperature for the 1-keV aurora is higher than for the 10-keV aurora, in spite of the 1-keV heating rate being smaller, because the heat produced by 1-keV electrons is deposited at a higher altitude above the IR cooling region. The low-latitude exospheric temperature deduced from Voyager UVS solar occultation data [*Broadfoot et al.*, 1981] is about 1100 K, considerably smaller than our calculated auroral temperatures, but considerably larger than our temperature calculated, including only solar heating processes.

The exospheric temperature in the auroral region is probably greater than it is at mid-latitudes; however, it is probably not as large as we have calculated here (Figure 16). The extremely large auroral heating rates we have

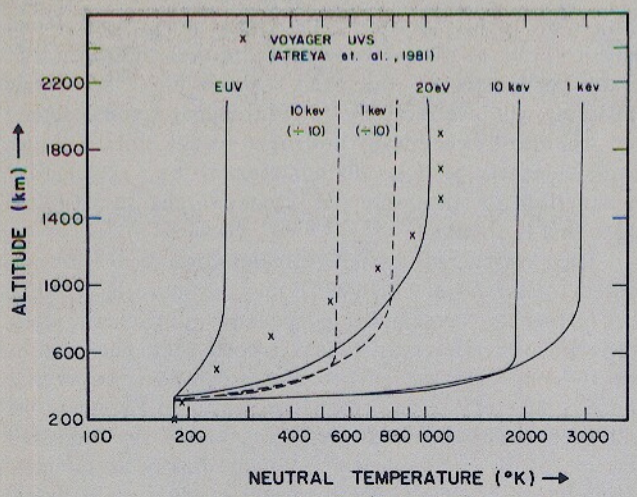

Fig. 16. Neutral temperature as a function of altitude for several cases of interest. The EUV results use only photoelectrons as a heat source. The 20-eV case considers the heating due to 20-eV electrons with an energy flux equal to 0.5 ergs $cm^{-2}s^{-1}$. The 1- and 10-keV auroral electron cases show the effects of electron heating from 1- and 10-keV electrons with an energy flux of 10 ergs cm^{-2} s^{-1} and for auroral heating rates diluted by a factor of 10 to illustrate the possible global effects of auroral heating. The Voyager UVS stellar occultation-derived profile is shown by the crosses.

calculated are actually lower limits to the true auroral heating rates, since we have not included Joule heating, which is probably very important at high latitudes [*Nishida and Watanabe*, 1981; *Waite*, 1981]. These very large auroral heat sources will certainly generate strong thermospheric winds that will globally redistribute both heat and neutral constituents like H. This thermospheric circulation will serve to supply lower latitudes with both heat and atomic hydrogen, as well as dilute the actual amount of heat and H remaining behind in the auroral zone. To simulate crudely the effects diluted auroral heating might have on the thermal structure, we have solved the heat conduction equation by using 1- and 10-keV heating rates decreased by a factor of 10, which is representative of a partial dilution of the auroral heat by horizontal transport out of the auroral regions. The resulting exospheric temperatures are 560 and 830 K for 10- and 1-keV electron beams, respectively (Figure 16). The temperatures are larger than the solar EUV produced temperatures, but smaller than the actual low-latitude temperature; however, we have not included all possible heat sources, and our basic approach is certainly oversimplified.

An alternative source of mid- and low-latitude heating may be low-latitude precipitation of low-energy electrons such as the 20-eV electrons discussed in the atomic hydrogen bulge section. The temperature profile for the 20-eV electron beam with a total energy flux of 0.5 ergs cm^{-2} s^{-1} is shown in Figure 16. The agreement of this temperature profile with the inferred thermospheric temperature profile of *Festou et al.* [1981] is surprisingly good. Thus, as in the case of atomic hydrogen, redistributed high-latitude heating as well as low-latitude soft electron precipitation may both be important sources of heating in the Jovian thermosphere.

5. IONOSPHERIC EFFECTS

We have calculated ion densities in the Jovian ionosphere for low- and mid-latitudes (including only photoionization and secondary ionization by photoelectrons) and for the auroral regions (including the additional particle impact ionization). Production rates for H^+ and H_2^+ are shown in section 3.

The chemical losses of H^+, used in standard models of the ionospheres of major planets [*Atreya and Donahue*, 1976; *Chen*, 1981], are three-body recombinations with H_2, reactions with CH_4, and radiative recombination. Using these loss processes, the calculated total electron density at the ionospheric peak resulting from auroral precipitation is of the order of 10^7 cm^{-3} (see Figure 17), which is 100 times greater than the values measured by the Voyager occultation experiment [*Eshleman et al.*, 1979]. These very large densities are a consequence of the large production of H^+ due to electron precipitation. It is clear that some other loss mechanism is necessary to explain the much lower measured densities. *McElroy* [1973] noted the possible importance of proton loss to vibrationally excited molecular hydrogen, and *Cravens* [1974], *Atreya et al.* [1979], and *Atreya and Donahue* [1982] discussed the increased significance of this mechanism owing to the possibility of considerably higher H_2 vibrational temperatures in the auroral zone. The reaction is

$$H^+ + H_2\ (v \geq 4) \rightarrow H_2^+ + H \qquad \text{(R2)}$$

followed by

$$H_2^+ + H_2 \rightarrow H_3^+ + H$$

$$H_3^+ + e \rightarrow H_2 + H,$$

which results in the loss of a proton. In the auroral zone, particle impact of electrons on H_2 should raise the vibrational temperature considerably [*Cravens*, 1974], and 'Treanor' pumping [*Treanor et al.*, 1968] can result in

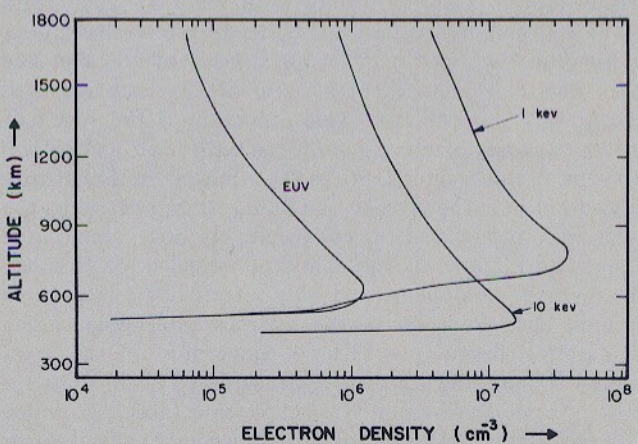

Fig. 17. Ionosphere electron density profiles as a function of altitude for a solar EUV produced ionosphere and the 1- and 10-keV auroral ionospheres ignoring the possible effects of the $H^+ + H_2$ ($v \geq 4$) reaction.

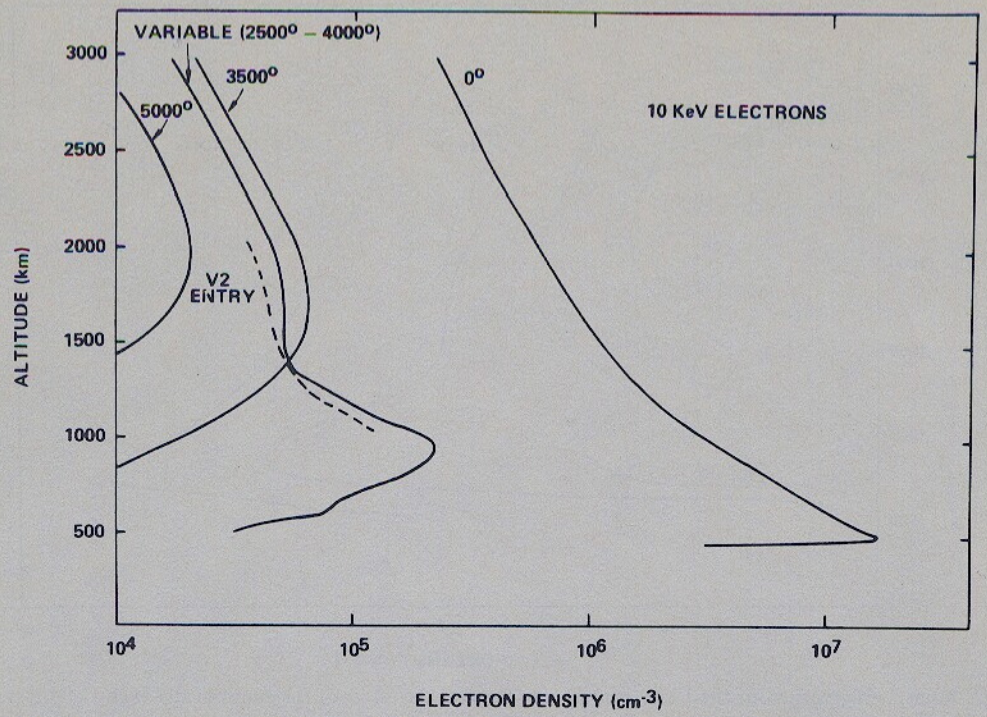

Fig. 18. Several ionospheric profiles for the 10-keV auroral case showing the possible effects of the reaction of $H^+ + H_2$ ($V \geq 4$). The V-2 entry electron density measurements taken at 66.7 latitude are shown by the dashed line.

highly skewed vibrational distributions. Tables 4–5 show that about 10% of the total incident auroral energy goes into vibrational excitation.

5.1. *Auroral Ionosphere*

We have tried two scenarios for the 10-keV aurora. First, we assumed altitude-independent vibrational temperatures (T_{vib}) equal to 0, 2500, and 5000 K. For the second scenario, we used a vibrational temperature profile that is constant with altitude below 1000 km and above 1500 km and increases linearly from 2500 to 4000 K between these two altitudes. The reaction rate for R2 was taken to be 10^{-9} cm^3 s^{-1}. The results for both scenarios are shown in Figure 18. It can be seen that when reaction R2 is not included (T_{vib} = 0 K), the electron density is much higher than the Voyager observation. Vibrational temperature distributions that are constant with altitude do reduce the densities but also tend to raise the height of the peak. Only when a variable temperature distribution is used does the calculated electron density distribution resemble the measurements. Lower vibrational temperatures can be expected at lower altitudes where the atmosphere is more dense because of the more rapid quenching of excited H_2 [*Cravens*, 1974].

We also tried these two scenarios for the 1-keV aurora and found that even with the variable vibrational temperature reaching a value as high as 8000 K the calculated electron density profile cannot be made to match the observation (Figure 19). The large H^+ production by 1-keV electrons at high altitudes is too much for the chemical loss, because the H_2 density is of the order of 10^8 cm^{-3} at topside altitudes whether vibrationally excited or not. The computational evidence presented here, then, favors higher primary energies for electrons (approximately 10 keV) and/or an increased thermospheric temperature so that most of the ionization occurs at atmospheric levels where reactions with the more plentiful H_2 may deplete the ions.

5.2. *Mid- and Low-Latitude Ionosphere*

At mid- and low-latitudes, it has been shown [*Chen*, 1982] that the atomic hydrogen density is important in determining the electron density profile. Using the relatively high values for H as calculated in this paper and in *Atreya et al.* [1981] and using solar EUV ionization as the only source, the ionospheric peak at mid- and low-Jovian latitude is calculated to be at 600 km with a value of 2.2×10^6 cm^{-3} (Figure 20). It was found that a high H_2 vibrational temperature will tend to raise the height of the peak, but Figure 20 shows that introducing a 2500 K vibrational temperature will increase the height of the peak only 500 km while decreasing the density of the peak far too much. However, if there is an additional ionization source present, particularly at higher altitudes, then the higher vibrational temperatures can raise the peak to an altitude and value close to the observation. This was done with an ion production rate approximately twice the solar EUV production rate; the peak was raised to 1800 km by using a 3000 K vibrational temperature (Figure 20). The additional atomic hydrogen and ion production needed in such a scenario could be produced by a low-energy electron precipitation source such as the 20-eV mid- and low-latitude electron precipitation source discussed in section 4. This precipitation would also provide the necessary vibrational heating. Thus, the current ionospheric measurements lend some support to a mid- and low-latitude low-energy

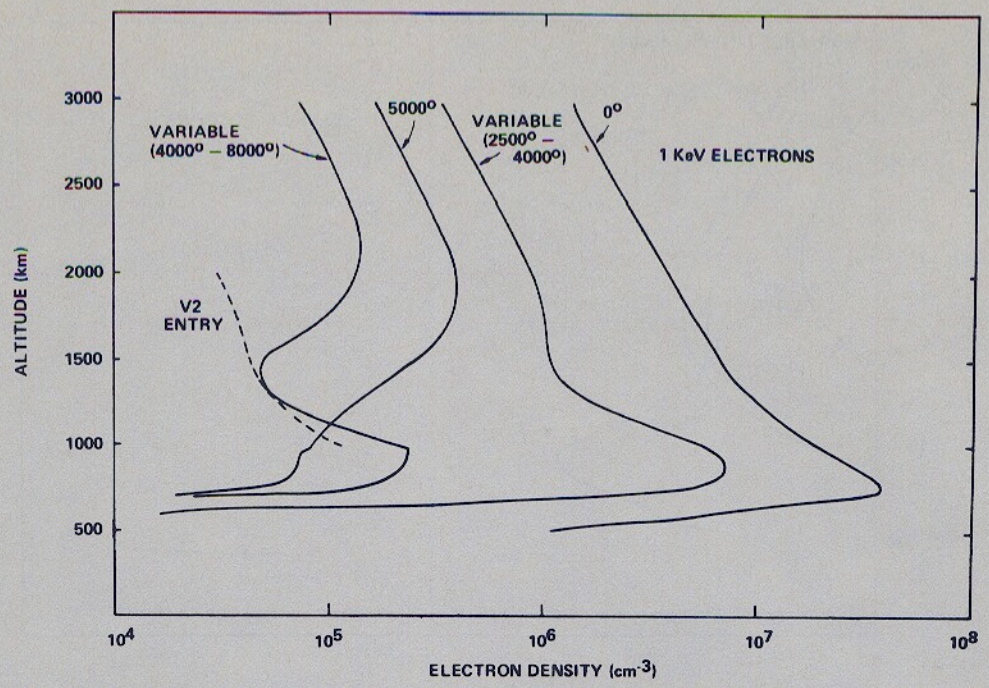

Fig. 19. Ionospheric profiles for the 1-keV auroral case showing the effect of the vibrationally excited H_2 loss process for H^+. The V-2 entry results are shown by the dashed line.

precipitation; the outstanding problem with this scenario is the observed day/night asymmetry of the Lyman and Werner bands.

5.3. Ionospheric Discussion

McConneil et al. [1982], following the earlier suggestions of *Atreya et al.* [1979] and *Atreya and Donahue* [1982], have suggested that a combination of vibrational heating of H_2 and vertical ionospheric drifts may explain the Jovian ionospheric observations. This parametric study provides reasonable fits to the data and may be an alternative and/or complementary theoretical ionospheric explanation. However, one distinct problem with their interpretation of the high-latitude ionosphere is the lack of any high-

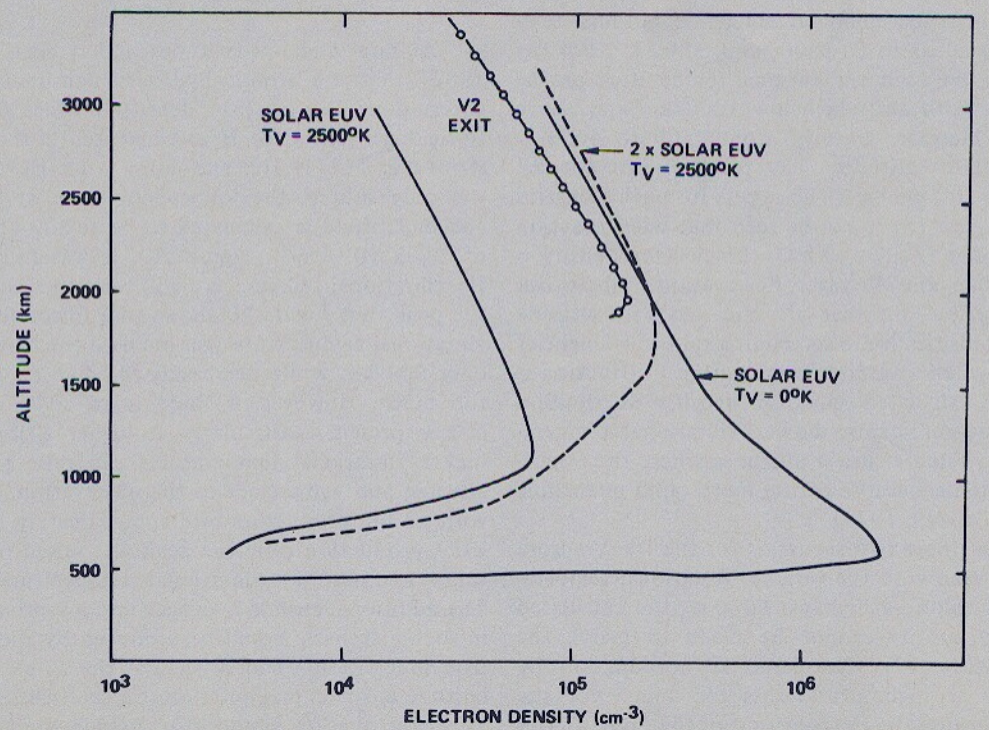

Fig. 20. Ionospheric density profiles for the mid-latitude Jupiter atmosphere. The effects of increased soft electron production of H and increased vibrational temperatures are illustrated. The V-2 exit radio occultation electron density measurements for mid-latitudes are shown by the dashed line.

latitude ionization source, which is extremely hard to ignore in light of the observed UVS airglow observations and the large corresponding ionization sources suggested by this study.

Our calculations show that for the auroral zone ionosphere, the loss of protons to vibrationally excited molecular hydrogen can account for the observations providing the H_2 vibrational temperature is variable with altitude and of the order of thousands of degrees. If the principal ionization source is an electron beam, then higher energy (10 keV) fluxes are more likely than lower energy (1 keV) fluxes. For the mid-latitude case, the complete theoretical analysis depends on observations of the lower ionosphere which are not yet available. However, the observed topside layer can be approximated if there is an additional ionization source about twice the value of the solar EUV source, an increased abundance of H, and the vibrational temperature of molecular hydrogen is of the order of 3000 K.

6. SUMMARY

We have presented a comprehensive theoretical model of both the auroral and nonauroral thermosphere and ionosphere of Jupiter. We have examined in some detail the deposition of energy in the upper atmosphere of Jupiter by solar extreme ultraviolet photons and by 1- and 10-keV precipitating electrons. An incident auroral electron flux of 10 ergs cm^{-2} s^{-1} will not only supply the Lyman and Werner band emissions required by the Voyager UVS measurements, but will also generate about 5 ergs cm^{-2} s^{-1} of heat and 4.7×10^{11} H atoms cm^{-2} s^{-1}, about 2 orders of magnitude more heat and H atoms than can be produced by absorption of EUV photons alone. We have also examined the energy deposition of very energetic (approximately 125 keV) and very soft (approximately 20 eV) electrons in the equatorial thermosphere.

We then considered the effects of the auroral and nonauroral energy deposition on the atmosphere and ionosphere. We have shown that energetic electrons cannot produce H atoms that can increase the solar resonance scattering of Lyman alpha in a localized region without also increasing Lyman and Werner band emissions from the region of precipitation. We also looked at the role that soft electron precipitation may play in determining the structure of the topside ionosphere at mid-latitudes. We calculated very large atomic hydrogen densities and neutral temperatures in the auroral region and discussed the role of vibrationally excited H_2 in controlling the electron density in the auroral ionosphere. We have suggested that aurorally produced atomic hydrogen possibly combined with mid-latitude soft electron precipitation might be responsible for the global distribution of atomic hydrogen in the Jovian upper atmosphere. Theoretical development of an aurorally driven thermospheric circulation model is needed to further understand the role that Jovian aurora play in global energetics and atomic hydrogen production.

Acknowledgments. We would like to acknowledge the National Center for Atmospheric Research for the computer resources grant, which was essential in development of the model and the subsequent model results, and NASA grants NSG-7404 and NAGW-15 from the NASA Planetary Atmospheres Program. We would also like to acknowledge the partial support of the NASA Jupiter Data Analysis Program (NAGW-312) and NASA grant NGR 23-005-015.

The Editor thanks D. Shemansky and another referee for their assistance in evaluating this paper.

REFERENCES

Ashihara, O., and M. Shimizu, The effect of electron precipitation on the Jovian ionosphere, *Astron. Astrophys., 57,* 85, 1977.

Atreya, S. K., and T. M. Donahue, Model ionospheres of Jupiter, in *Jupiter,* edited by T. Gehrels, pp. 304-318, University of Arizona Press, Tucson, 1976.

Atreya, S. K., and T. M. Donahue, Models of the Jovian upper atmosphere, *Rev. Geophys. Space Phys., 17,* 338, 1979.

Atreya, S. K., and T. M. Donahue, The atmosphere and ionosphere of Jupiter, *Vistas Astron., 25,* 315, 1982.

Atreya, S. K., Y. L. Yung, T. M. Donahue, and E. S. Barker, Search for Jovian auroral hot spots, *Astrophys. J., 218,* L83-L87, 1977.

Atreya, S. K., T. M. Donahue, and J. H. Waite, Jr., An interpretation of the Voyager measurements of Jovian electron density profiles, *Nature, 280,* 795-796, 1979.

Atreya, S. K., T. M. Donahue, and M . C. Festou, Jupiter: Structure and composition of the upper atmosphere, *Astrophys. J., 247,* L43, 1981.

Atreya, S. K., T. M. Donahue, M. C. Festou, R. B. Kerr, J. L. Bertaux, E. S. Barker, W. D. Cochran, and W. L. Upson, II, Copernicus measurement of the Jovian Lyman alpha emission, and its aeronomical significance, *Astrophys. J., 262,* 377-387, 1982.

Bagenal, F., and J. D. Sullivan, Direct plasma measurements in the Io torus and inner magnetosphere of Jupiter, *J. Geophys. Res., 86,* 8447, 1981.

Banks, P. M., and A. F. Nagy, Concerning the influence of elastic scattering upon photoelectron transport and escape, *J. Geophys. Res., 75,* 1902, 1970.

Barbosa, D. D. F. L. Scarf, W. S. Kurth, and D. A. Gurnett, Broadband electrostatic noise and field-aligned currents in Jupiter's middle magnetosphere, *J. Geophys. Res., 86,* 8357, 1981.

Bates, D. R., and A. Dalgarno, Electronic Recombination, in *Atomic and Molecular Processes,* edited by D. R. Bates, Academic, New York, 1962.

Bridge, H. S., J. W. Bekher, A. J. Lazarus, J. D. Sullivan, R. L. McNutt, F. Bagenal, J. D. Scudder, E. C. Sittler, G. L. Siscoe, V. N. Vasyliunas, C. K. Goertz, and C. M. Yeates, Magnetic field studies at Jupiter by Voyager 1: Preliminary results, *Science, 204,* 982, 1979.

Broadfoot, A. L., M. J. S. Belton, P. Z. Takacs, B. R. Scandel, D. E. Shemansky, J. B. Holbert, J. M. Ajello, S. K. Atreya, T. M. Donahue, H. W. Moos, J. L. Bertaux, J. E. Blamont, D. F. Strobel, J. C. McConnell, A. Dalgarno, R. Goody, and M. B. McElroy, Extreme ultraviolet observations from Voyager 1 encounter with Jupiter, *Science, 204,* 979, 1979.

Broadfoot, A. L., B. R. Sandel, D. E. Shemansky, J. C. McConnell, G. R. Smith, J. B. Holberg, S. K. Atreya, T. M. Donahue, D. F. Strobel, and J. L. Bertaux, Overview of the Voyager ultraviolet spectrometer results through Jupiter encounter, *J. Geophys. Res., 86,* 8259, 1981.

Chen, R. H., Studies of Jupiters lower ionospheric layers, *J. Geophys. Res., 86,* 7792, 1981.

Chen, R. H., Time dependent calculations of Jupiter's ionosphere, *J. Geophys. Res., 87,* 167, 1982.

Clarke, J. T., H. W. Moos, S. K. Atreya, and A. L. Lane, Observations from earth orbit and variability of the polar aurora on Jupiter, *Astrophys. J., 241,* 179-182, 1980.

Cook, G. R., and P. H. Metzger, Photoionization and absorption cross sections of H_2 and D_2 in the vacuum ultraviolet region, *J. Opt. Soc. Am., 54,* 968-972, 1964.

Coroniti, F. V., F. L. Scarf, C. F. Kennel, W. S. Kurth, and D. A. Gurnett, Detection of Jovian whistler mode chorus: Implications for the Io torus aurora, *Geophys. Res. Lett., 7,* 45, 1980.

Cravens, T. E., Astrophysical applications for electron energy deposition in molecular hydrogen, Ph.D. thesis, Harvard Univ., Cambridge, Mass., 1974.

Cravens, T. E., and A. I. Stewart, Global morphology of nitric oxide in the lower E region, *J. Geophys. Res., 83,* 2446, 1978.

Cravens, T. E., G. A. Victor, and A. Dalgarno, The absorption of energetic electrons by molecular hydrogen gas, *Planet. Space Sci., 23,* 1059, 1975.

Cravens, T. E., J. C. Gerard, A. I. Stewart, and D. W. Rusch, The latitudinal gradient of nitric oxide in the thermosphere, *J. Geophys. Res., 84,* 2675, 1979.

de Heer, F. J., and J. D. Carriere, Emission of the Werner band system and Lyman alpha radiation for 0.05-6-keV electrons in H_2, *J. Chem. Phys., 55,* 3829, 1971.

Dessler, A. J., B. R. Sandel, and S. K. Atreya, The Jovian hydrogen bulge: Evidence for corotating magnetospheric convection, *Planet. Space Sci., 29, 215, 1981.*

Dulk, G. A., J. A. Eddy, and J. P. Emerson, Search for visual auroral on Jupiter, *Astrophys. J., 159,* 1123–1124, 1970.

Eshleman, V. R., G. L. Tyler, G. E. Wood, G. F. Lindal, J. D. Anderson, G. S. Levy, and T. A. Croft, Radio science with Voyager 1 at Jupiter: Preliminary profiles of the atmosphere and ionosphere, *Science, 204,* 976–978, 1979.

Festou, M. F., S. K. Atreya, T. M. Donahue, B. R. Sandel, D. E. Shemansky, and A. L. Broadfoot, Composition and thermal profiles of the Jovian upper atmosphere determined by the Voyager stellar occultation experiment, *J. Geophys. Res., 86,* 5715, 1981.

Garvey, R. H., H. S. Porter, and A. E. S. Green, Relativistic yield spectra for H_2, *J. Appl. Phys., 48,* 4353, 1977.

Gehrels, N., E. C. Stone, and J. H. Trainor, Energetic oxygen and sulfur ions in the Jovian magnetosphere, *J. Geophys. Res., 86,* 8906, 1981.

Gerard, J.-C., and V. Singh, A model of energy deposition of energetic electrons and EUV emission in the Jovian and Saturnian atmospheres, *J. Geophys. Res., 87,* 4525, 1982.

Gerhart, D. E., Comprehensive optical and collision data for radiation action, 1, H_2, *J. Chem. Phys., 62,* 821, 1975.

Giles, J., H. W. Moos, and W. R. McKinney, The far ultraviolet (1200–1900 Å) spectrum of Jupiter obtained with a rocket-borne multichannel spectrometer, *J. Geophys. Res., 81,* 5797, 1976.

Goertz, C. K., Proton aurora on Jupiter's nightside, *Geophys. Res. Lett., 7,* 365–368, 1980.

Gurnett, D. A., W. S. Kurth, and F. L. Scarf, Plasma wave observations near Jupiter: Initial results from Voyager 2, *Science, 206,* 987, 1979.

Hanel, R., B. Conrath, M. Flasar, L. Herath, V. Kunde, P. Lowman, W. MacGuire, J. Pearl, J. Pirraglia, R. Samuelson, D. Gautier, P. Gierasch, L. Horn, S. Kumar, and C. Ponnamperuma, Infrared observations of the Jovian system from Voyager 2, *Science, 206,* 952, 1979.

Hanley, H. J. M., R. D. McCarty, and H. Inteman, The viscosity and thermal conductivity of dilute gaseous hydrogen from 15 to 5000 K, *J. Res. Natl. Bur. Stand., 74A,* 331, 1970.

Heaps, M. G., The roles of particle precipitation and Joule heating in the energy balance of the Jovian thermsophere, *Icarus, 29,* 273–281, 1976.

Heaps, M. G., J. N. Bass, and A. E. S. Green, Electron excitation of a Jovian aurora, *Icarus, 20, 297–303, 1973.*

Heroux, L., and H. E. Hinteregger, Aeronomical reference spectrum for Solar UV below 2000 A, *J. Geophys. Res., 83,* 5305, 1978.

Hunten, D. M., and A. J. Dessler, Soft electrons as a possible heat source for Jupiter's thermosphere, *Planet. Space Sci., 25,* 817–821, 1977.

Hunter, J. H., H auroral activity of Jupiter, *Nature, 223,* 388–389, 1969.

Jackman, C. H., R. H. Garvey, and A. E. S. Green, Electron impact on atmospheric gases, 1, Updated cross sections, *J. Geophys. Res., 82,* 5081, 1977.

Krimigis, S. M., T. P. Armstrong, W. S. Axford, C. P. Bostrom, C. Y. Fan, G. Gloeckler, L. J. Lanzerotti, E. P. Kearth, R. D. Zwickl, J. F. Carbary, and D. C. Hamilton, Low-energy charged particle environment at Jupiter: A first look, *Science, 204,* 998, 1979.

Kurth, W. S., D. D. Barbosa, D. A. Gurnett, and F. L. Scarf, Electrostatic waves in the Jovian magnetosphere, *Geophys. Res. Lett., 7,* 57, 1980.

Leu, M. T., M. A. Biondi, and R. Johnson, Dossociative recombination of electrons with H3+ and H5+ ions, *Phys. Rev., 8,* 413, 1973.

McConnell, J. C., J. B. Holberg, G. R. Smith, B. R. Sandel, D. E. Shemansky, and A. L. Broadfoot, A new look at the ionosphere of Jupiter in light of the UVS occultation results, *Planet. Space Sci., 30,* 151, 1982.

McElroy, M. B., The ionospheres of the major planets, *Space Sci. Rev., 14,* 460–473, 1973.

Miles, W. T., R. Thompson, and A. E. S. Green, Electron impact cross sections and energy deposition in molecular hydrogen, *J. Appl. Phys., 43,* 678, 1972.

Moiseiwitsch, B. L., Elastic scattering of electrons, *Atmos. Mol. Process.,* 280, 1962.

Nagy, A. F., and P. M. Banks, Photoelectron fluxes in the ionosphere, *J. Geophys. Res., 75,* 6260, 1970.

Nishida, A., and Y. Watanabe, Joule heating of the Jovian ionosphere by corotation enforcement currents, *J. Geophys. Res., 86,* 9945, 1981.

Olivero, J. J., J. N. Bass, and A. E. S Green, Photoelectron excitation of the Jupiter dayglow, *J. Geophys. Res., 78,* 2812, 1973.

Sandel, B. R., D. E. Shemansky, A. L. Broadfoot, J. L. Bertaux, J. E. Blamont, M. J. S. Belton, J. M. Ajello, J. B. Holberg, S. K. Atreya, T. M. Donahue, H. W. Moos, D. F. Strobel, J. C. McConnell, A. Dalgarno, R. Goody, M. B. McElroy, and P. Z. Takacs, Extreme ultraviolet observation from Voyager 2 encounter with Jupiter, *Science, 206,* 962–966, 1979.

Sandel, B. R., A. L. Broadfoot, and D. F. Strobel, Discovery of a longitudinal asymmetry in the hydrogen Lyman-alpha brightness of Jupiter, *Geophys. Res. Lett., 1,* 5, 1980.

Scarf, F. L., D. A. Gurnett, and W. S. Kurth, Jupiter plasma wave observations: An initial Voyager 1 overview, *Science, 204,* 991, 1979.

Schwitters, M. J., A search for Jovian limb aurora, *Icarus, 9,* 570–573, 1968.

Shyn, T. W., and W. E. Sharp, Double differential cross sections of secondary electrons ejected from gases by electron impact: 25–250 eV on H_2 (abstract), *Eos Trans. AGU, 61,* 285, 1980.

Shyn, T. W., and W. E. Sharp, Angular distribution of electrons elastically scattered from H_2, *Phys. Rev. A, 24,* 1734, 1981.

Spindler, R. J., Jr., Franck-Condon factors for the band systems of molecular hydrogen, 1, The ($B^1\Sigma_u^+$-$X^1\Sigma_u^+$), ($I^1\pi_g$-$B^1\Sigma_u^+$), and ($d^3\Sigma_g^+$-$a^3\Sigma_g^+$) systems, *J. Quant. Spectrosc. Radiat. Transfer, 9,* 597, 1969*a*.

Spindler, R. J., Jr., Franck-Condon factors for the band systems of molecular hydrogen, 2, the ($C^1\pi_g$-$X^1\Sigma_g^+$), ($D^1\pi_u$-$X^1\Sigma_g^+$) and ($h^3\Sigma_g^+$-$c^3\pi_u$) systems, *J. Quant. Spectrosc. Radiat. Transfer, 9,* 627, 1969*b*.

Srivastava, S. K., and S. Jensen, Experimental differential and integral electron impact cross sections for the $B^1\Sigma_u^+$ state in H_2 in the intermediate-energy region, *J. Phys. B, 10,* 3341, 1977.

Stone, E. J., and E. C. Zipf, Excitation of the Werner bands of H_2 by electron impact, *J. Chem. Phys., 56, 4646, 1972.*

Strobel, D. F., The photochemistry of methane in the Jovian atmosphere, *J. Atmos. Sci., 26,* 906, 1969.

Strobel, D. F., The photochemistry of hydrocarbons in the Jovian atmosphere, *J. Atmos. Sci., 30,* 489, 1973.

Strobel, D. F., Aeronomy of the major planets: Photochemistry of ammonia and hydrocarbons, *Rev. Geophys. Space Phys. 13,* 372, 1975.

Strobel, D. F., and G. R. Smith, On the temperature of the Jovian thermosphere, *J. Atmos. Sci., 30,* 718–725, 1973.

Swartz, W. E., J. S. Nisbet, and A. E. S. Green, Analytic expression for the energy transfer rate from photoelectrons to thermal electrons, *J. Geophys. Res., 76,* 8425, 1971.

Theard, L. P., and W. T. Huntress, Jr., Ion molecule reactions and vibrational deactivation of H_2^+ ions in mixtures of hydrogen and helium, *J. Chem. Phys., 60,* 2840, 1974.

Thorne, R. M., Jovian auroral secondary electrons and their influence on the Io plasma torus, *Geophys. Res. Lett., 8,* 509, 1981*a*.

Thorne, R. M., Microscopic plasma processes in the Jovian magnetosphere, in *Physics of the Jovian Magnetosphere,* chapter 12, edited by A. J. Dessler, Cambridge University Press, New York, 1981*b*.

Thorne, R. M., and B. J. Tsurutani, Diffuse Jovian aurora influenced by plasma injection from Io, *Geophys. Res. Lett., 6,* 649, 1979.

Treanor, C. E., J. W. Rich, and R. G. Rehm, Vibrational relaxation

of anharmonic oscillators with exchange-dominated collisions, *J. Chem. Phys., 48,* 1798, 1968.

Vogt, R. E., W. R. Cook, A. C. Cummings, T. L. Garrard, N. Gehrels, E. C. Stone, J. H. Trainor, A. W. Schardt, T. Conlon, N. Cal, and F. B. McDonald, Voyager 1: Energetic ions and electrons in the Jovian magnetosphere, *Science, 204,* 1003, 1979.

Waite, J. H., Jr., The ionosphere of Saturn, Ph.D. thesis, Univ. of Mich., Ann Arbor, 1981.

Waite, J. H., Jr., and T. E. Cravens, Vibrational and rotational cooling of electrons by molecular hydrogen, *Planet. Space Sci., 29,* 1333, 1981.

Waite, J. H., Jr., T. E. Cravens, S. K. Atreya, J, Kozyra, and A. F. Nagy, A model of the Jovian aurora (abstract), *Eos Trans. AGU, 61,*1024, 1980.

Yung, Y. L., and D. F. Strobel, Hydrocarbon photochemistry and Lyman alpha albedo of Jupiter, *Astrophys. J., 239,* 395, 1980.

Yung, Y. L., G. R. Gladstone, K. M. Chang, J. M. Ajello, and S. K. Srivastava, H_2 fluorescence spectrum from 1200 to 1700 Å by electron impact: Laboratory study and application to Jovian aurora, *Astrophys. J., 254,* L65, 1982.

(Received September 28, 1982;
revised January 31, 1983;
accepted February 1, 1983.)